

RESEARCH ARTICLE

10.1029/2019EF001469

Insights From CMIP6 for Australia's Future Climate



Key Points:

- CMIP6 shows incremental improvement of the simulation of Australian climate compared to CMIP5
- CMIP6 climate projections are similar to CMIP5 except for a group of higher sensitivity models with warmer projected change

Supporting Information:

- Figure S1

Correspondence to:

M. R. Grose,
michael.grose@csiro.au

Citation:

Grose, M. R., Narsey, S., Delage, F. P., Dowdy, A. J., Bador, M., Boschat, G., et al. (2020). Insights from CMIP6 for Australia's future climate. *Earth's Future*, 8, e2019EF001469. <https://doi.org/10.1029/2019EF001469>

Received 24 DEC 2019

Accepted 1 APR 2020










Accepted article online 08 APR 2020

Author Contributions:

Conceptualization: M. R. Grose

Formal analysis: G. Boschat

Writing - original draft: M. R. Grose, G. Boschat

M. R. Grose¹ , S. Narsey² , F. P. Delage² , A. J. Dowdy² , M. Bador³ , G. Boschat^{2,4} , C. Chung² , J. B. Kajtar⁵ , S. Rauniyar² , M. B. Freund⁶ , K. Lyu^{1,7} , H. Rashid⁸ , X. Zhang¹ , S. Wales³ , C. Trenham⁹ , N. J. Holbrook⁵ , T. Cowan^{2,10} , L. Alexander³ , J. M. Arblaster⁴ , and S. Power²

¹CSIRO Oceans and Atmosphere, Hobart, Australia, ²Australian Bureau of Meteorology, Melbourne, Australia,

³University of Melbourne and ARC Centre of Excellence for Climate Extremes, Melbourne, Australia, ⁴Monash University and ARC Centre of Excellence for Climate Extremes, Melbourne, Australia, ⁵Institute for Marine and Antarctic Studies and ARC Centre of Excellence for Climate Extremes, University of Tasmania, Hobart, Australia, ⁶CSIRO Agriculture and Food, Hobart, Australia, ⁷Centre for Southern Hemisphere Oceans Research, Hobart, Australia, ⁸CSIRO Oceans and Atmosphere, Melbourne, Australia, ⁹CSIRO Oceans and Atmosphere, Canberra, Australia, ¹⁰Centre for Applied Climate Sciences, University of Southern Queensland, Toowoomba, Australia

Abstract Outputs from new state-of-the-art climate models under the Coupled Model Inter-comparison Project phase 6 (CMIP6) promise improvement and enhancement of climate change projections information for Australia. Here we focus on three key aspects of CMIP6: what is new in these models, how the available CMIP6 models evaluate compared to CMIP5, and their projections of the future Australian climate compared to CMIP5 focussing on the highest emissions scenario. The CMIP6 ensemble has several new features of relevance to policymakers and others, for example, the integrated matrix of socioeconomic and concentration pathways. The CMIP6 models show incremental improvements in the simulation of the climate in the Australian region, including a reduced equatorial Pacific cold tongue bias, slightly improved rainfall teleconnections with large-scale climate drivers, improved representation of atmosphere and ocean extreme heat events, as well as dynamic sea level. However, important regional biases remain, evident in the excessive rainfall over the Maritime Continent and rainfall pattern biases in the nearby tropical convergence zones. Projections of Australian temperature and rainfall from the available CMIP6 ensemble broadly agree with those from CMIP5, except for a group of CMIP6 models with higher climate sensitivity and greater warming and increase in some extremes after 2050. CMIP6 rainfall projections are similar to CMIP5, but the ensemble examined has a narrower range of rainfall change in austral summer in Northern Australia and austral winter in Southern Australia. Overall, future national projections are likely to be similar to previous versions but perhaps with some areas of improved confidence and clarity.

1. Introduction

The new Coupled Model Inter-comparison Project phase 6 (CMIP6) multimodel ensemble (Eyring et al., 2016) builds upon the previous phase 5 (Taylor et al., 2012) and enables new opportunities to examine the climate system and make regional projections of the climate under future scenarios, including for Australia. CMIP6 includes coupled atmosphere-ocean general circulation model (AOGCM) and Earth system model (ESM) simulations of the global climate, taken together under the umbrella term global climate model (GCM). Previous CMIP ensembles have been used as inputs to the Intergovernmental Panel on Climate Change (IPCC) fourth and fifth assessment reports, AR4 and AR5 (IPCC, 2007; IPCC, 2013), and as the main inputs to Australian national climate projections, complemented by dynamical and statistical downscaling (CSIRO and Bureau of Meteorology, 2007; CSIRO and Bureau of Meteorology, 2015). The new CMIP6 ensemble will be of strong interest for both assessing climate change processes as part of the sixth IPCC assessment report (AR6) and for producing updated national climate change projections for Australia, as well as providing new insights into the climate system and climate change relevant to the region.

CMIP6 will provide value for producing national climate projections products for Australia in three main areas. First, CMIP6 projections are conducted under a new framework of socioeconomic as well as emissions pathways, with some GCMs including climate processes and earth system elements that were not included in previous generations. Second, any improvement in the evaluation of these models against the observed climate may lead to increased confidence in certain climate projections. Third, any different future

© 2020. The Authors.

This is an open access article under the terms of the Creative Commons Attribution-NonCommercial-NoDerivs License, which permits use and distribution in any medium, provided the original work is properly cited, the use is non-commercial and no modifications or adaptations are made.

projections in CMIP6 compared to CMIP5 are of strong interest for the world, and for Australia. This includes cases where there is increased model agreement of constrained ranges of projected change or conversely where projected changes from CMIP6 are outside the CMIP5 range for a given forcing scenario.

One important new attribute of CMIP6 is the presence of a group of models with higher climate sensitivity than in CMIP5 (NCC Editorial, 2019). The equilibrium climate sensitivity (ECS), also referred to as effective climate sensitivity, is defined as the estimated equilibrium global mean surface temperature change for a doubling of carbon dioxide concentration and calculated from abrupt $4\times\text{CO}_2$ simulations using the Gregory et al. (2004) method. Various lines of evidence were used in the IPCC AR5 to estimate that ECS is in the *likely* range 1.5 to 4.5 °C with a <5% chance of being 6 °C or more, and this range has been fairly consistent for over 25 years (Collins et al., 2013). The CMIP5 models, one line of evidence incorporated into the IPCC assessed range, had ECS in the range 2.6 to 4.6 °C, whereas CMIP6 contains numerous models with an ECS over 4.6 °C (Voosen, 2019). High sensitivity is expected to produce hotter temperature projections and greater changes in temperature extremes as well as some other climate variables for the globe and for Australia for a given scenario. The cause of the higher ECS is currently under investigation, but analysis of a few models suggests that stronger cloud feedbacks are one key factor (Gettelman et al., 2019; Forster et al., 2019). Currently, the ECS cannot be reliably constrained by observed trends (Gregory et al., 2019), and high values cannot be ruled out. Therefore, we do not make any decision whether the ECS values are implausible and to reject models on this basis, but rather we present all available results. Also of note is that a number of models (e.g., Sellar et al., 2019) have stronger than observed cooling during the period of strong aerosol forcing (1950s–1970s), which may then be relevant to the temperature projection.

Here we examine the available CMIP6 ensemble as it relates to producing climate projections for Australia. This study includes a discussion of the three aspects above: what is new in the models (discussed in section 2), how CMIP6 models evaluate compared to previous generations, and the CMIP6 projections of the future climate. The CMIP6 ensemble does not contain a full set of models yet, and may not do so for some time, so the model results considered here are not a full ensemble. Instead we present available CMIP6 simulations against the range of CMIP5 simulations, to see if the new models show any systematic improvements or provide projections that are outside of the CMIP5 range.

2. Data and Methods

2.1. New Features of the CMIP6 Database Relevant to Australian Climate Projections

The main focus of this study is on the new simulations of the future climate under scenarios of human emissions, referred to as ScenarioMIP (O'Neill et al., 2016). There are important new developments in ScenarioMIP compared to CMIP5, but there are also features of the other MIPs that are relevant as well.

Simulations in CMIP5 were made under a set of scenarios of anthropogenic greenhouse gas and aerosol concentrations resulting in different levels of radiative forcing—the Representative Concentration Pathways (RCPs) outlined in van Vuuren et al. (2011). Each ScenarioMIP simulation in CMIP6 is made under a combination of an RCP and a Shared Socioeconomic Pathway (SSP), outlined in Meinshausen et al. (2019), named for the SSP value then the RCP value. The RCPs, defined by the magnitude of enhanced radiative forcing at 2100, contain the same values as for CMIP5 but include some new ones: 1.9, 2.6, 3.4, 4.5, 6.0, 7.0, and 8.5 W m^{-2} . The five SSPs are summarized by the narrative headlines; SSP1—sustainability: taking the green road; SSP2—middle of the road; SSP3—regional rivalry: a rocky road; SSP4—inequality: a road divided; and SSP5—fossil-fuelled development: taking the highway. At the time of writing, and possibly for some time to come, outputs are only available for the “Tier 1” combinations: SSP1-26, SSP2-45, SSP3-70, and SSP5-85.

The framing by both SSP and RCP dimensions provides new opportunities to examine the future in terms of physical climate change and global socioeconomic pathways, including the interactions between the two.

There are also important new developments in other MIPs that are relevant to understanding climate variability and change in Australia and producing projections that are not discussed in this paper. These include decadal prediction (DCPP); high spatial resolution simulations (HighResMIP); coordinated regional downscaling experiment (CORDEX); vulnerability, impacts, adaptation, and climate services advisory board (VIACS AB); Geoengineering (GeoMIP); detection and attribution (DAMIP); and paleoclimate simulations (PMIP). In the fullness of time, the outputs of these MIPs, and the insights derived from them, will be of

potential interest and value in understanding climate processes in Australia and producing national climate projections for Australia.

2.2. Methods

This study uses one simulation each from a group of 33 CMIP6 models that are available at the time of writing (Table 1). A different set of models were available for each analysis, with Historical simulations from 27 models for the evaluation of temperature and rainfall, 15 models for the evaluation of marine heatwaves (MHWs), 20 models for projections of temperature, 16 for projections of mean rainfall, 12 models for the evaluation of extremes indices, and only seven for the evaluation and projections of extremes. The main focus for projections is on the SSP5-85 experiments, as this provides the strongest climate change signal, no inference about the likelihood of this SSP compared to others is made.

Table 1
CMIP6 Models and Simulations Used in This Study and Their Use in Each Analysis in the Paper

Model name	Run used	Mean Eval.	MHW	DSL	Temp.	Rainfall	Extr. Eval.	Extr. Proj.	Atmos. Lat/lon grid (°)	Ocean Lat/lon grid (°)	ECS (°C)	Aus proj 2090 SSP5-85 (°C)
1	ACCESS-CM2	r1i1p1f1	○	○	○	○	○	○	1.2 × 1.8	1.0 × 0.7	4.7	5.8
2	ACCESS-ESM-1-5	r1i1p1f1	○	○	○	○	○	○	1.2 × 1.8	1.0 × 0.7	3.9	4.6
3	AWI	r1i1p1f1			○				0.9 × 0.9			4.1
4	BCC-CSM2-MR	r1i1p1f1	○	○	○	○	○	○	1.1 × 1.1	1.0 × 0.7	3.1	3.5
5	BCC-ESM 1	r1i1p1f1	○	○			○		2.8 × 2.8	1.0 × 0.7	3.3	
6	CAMS-CSM1-0	r1i1p1f1	○			○			1.1 × 1.1		2.3	2.7
7	CanESM5	r1i1p1f1	○	○	○	○	○	○	2.8 × 2.8	1.0 × 0.8	5.6	6.3
8	CESM2	r1i1p1f1	○	○	○	○	○	○	0.9 × 1.3	1.1 × 0.4	5.2	5.2
9	CESM2-WACCM	r1i1p1f1	○		○	○	○	○	0.9 × 1.3		4.7	5.8
10	CNRM-CM6-1	r1i1p1f2	○	○	○	○	○	○	1.4 × 1.4	1.0 × 0.8	4.8	5.8
11	CNRM-CM6-1-HR	r1i1p1f2		○					~0.5	~0.25		
12	CNRM-ESM 2-1	r1i1p1f2	○	○	○	○	○	○	1.4 × 1.4	1.0 × 0.8	4.8	5.0
13	E3SM-1-0	r1i1p1f1			○				0.7 × 0.7		5.3	5.3
14	EC-Earth3	r2i1p1f1		○					0.7 × 0.7	1.0 × 0.8	4.2	
15	EC-Earth3-Veg	r1i1p1f1	○	○	○	○			0.7 × 0.7	1.0 × 0.8	4.3	4.3
16	FGOALS-g3	r1i1p1f1	○						2.3 × 2.0			
17	GFDL-CM4	r1i1p1f1	○	○	○	○	○	○	1.0 × 1.3	0.3 × 0.2	3.9	4.0
18	GFDL-ESM 4	r1i1p1f1	○						1.0 × 1.3		2.7	
19	GISS-E2-1-G	r1i1p1f1		○					2.0 × 2.5		2.4	
20	GISS-E2-1-G-CC	r1i1p1f1	○						2.0 × 2.5			
21	GISS-E2-1-H	r1i1p1f1	○						2.0 × 2.5		3.1	
22	HadGEM3-GC3.1	r1i1p1f3		○	○					1.0 × 0.8	5.5	
23	INM-CM4-8	r1i1p1f1		○	○				1.5 × 2.0		1.8	3.0
24	INM-CM5-0	r1i1p1f1		○	○				1.5 × 2.0		1.9	3.1
25	IPSL-CM6A-LR	r1i1p1f1	○		○	○	○	○	1.3 × 2.5	1.0 × 0.8	4.5	5.2
26	MCM-UA-1-0	r1i1p1f1	○						2.2 × 3.8		3.6	
27	MIROC6	r1i1p1f1	○		○	○			1.4 × 1.4		2.6	3.4
28	MIROC-ESM 2L	r1i1p1f1	○		○	○			2.7 × 2.8		2.7	3.3
29	MPI-ESM 1-2-HR	r1i1p1f1		○					~0.9	~0.4		
30	MPI-ESM 1-2-LR	r1i1p1f1		○					~2.0	~0.4		
31	MRI-ESM 2-0	r1i1p1f1	○		○	○	○	○	1.1 × 1.1		3.2	4.2
32	NESM3	r1i1p1f1	○	○	○				1.9 × 1.9	1.0 × 0.8	4.7	
33	NorCPM1	r1i1p1f1	○						1.9 × 2.5			
34	NorESM2-LM	r1i1p1f1	○		○		○		1.9 × 2.5	1.0 × 0.5	2.5	
35	NorESM2-MM	r1i1p1f1		○								
36	SAM0-UNICON	r1i1p1f1	○	○			○		0.9 × 1.3	1.1 × 0.4	3.6	
37	UKESM1-0-LL	r1i1p1f2	○	○	○	○	○	○	1.3 × 1.9	1.0 × 0.8	5.3	6.2

Note. Evaluation of means in Figures 1–6 (Eval.), dynamic sea level evaluation and projection (DSL), marine heatwave evaluation (MHW), temperature projection in Figure 8 (Temp.), rainfall projection in Figures 9 and 10 (Rainfall), evaluation of extremes (Extr. Eval.), and analysis of daily extremes in Figure 11 (Extremes). Also shown are the models' atmospheric spatial resolution, their reported effective climate sensitivity (ECS), and projection of Australian mean annual temperature between 1995–2014 and 2080–2099 under SSP5-85.

We compare the CMIP6 ensemble to up to 47 CMIP5 models for historical and RCP8.5 simulations (Table 2). The RCPs and SSPs are both defined by the enhanced radiative forcing, but have some differences. For example, while RCP8.5 and SSP5-85 both reach 8.5 W m^{-2} enhanced radiative forcing by 2100, the proportion of different greenhouse gases and aerosol pathways are different. Discrepancies in the forcing scenarios used will create some differences in the projections that are unrelated to the model behavior.

Table 2
CMIP5 Models Used, Details as for Table 1

	Run used	Eval.	MHW	Temp.	Rainfall	Extremes	Atmos. Lat/lon grid (°)	Ocean Lat/lon grid (°)	ECS (°C)	Aus proj 2090 RCP85 (°C)
1	ACCESS-1.0	rlilp1	0	0	0	0	1.3 × 1.9	1.0 × 0.7	3.8	4.5
2	ACCESS-1.3	rlilp1	0	0	0	0	1.3 × 1.9	1.0 × 0.7		4.6
3	BCC-CSM1-1	rlilp1	0	0	0	0	2.8 × 2.8	1.0 × 0.7		3.2
4	BCC-CSM1-1-m	rlilp1	0	0	0	0	2.8 × 2.8	1.0 × 0.7		3.1
5	BNU-ESM	rlilp1	0	0	0	0	2.8 × 2.8	1.0 × 0.9		3.9
6	CanESM2	rlilp1	0	0	0	0	2.8 × 2.8	1.4 × 0.9	3.7	4.9
7	CCSM4	rlilp1	0	0	0	0	0.9 × 1.3	1.1 × 0.4		3.5
8	CESM1-BGC	rlilp1	0	0	0	0	0.9 × 1.2	1.1 × 0.6		3.6
9	CESM1-CAM5	rlilp1	0	0	0	0	0.9 × 1.3	1.1 × 0.6	4.3	4.1
10	CESM1-CAM5-1-FV2	rlilp1	0	0	0	0	0.9 × 1.3	1.1 × 0.6		
11	CESM1-FASTCHEM	rlilp1	0	0	0	0	0.9 × 1.3	1.1 × 0.6		
12	CESM1-WACCM	rlilp1	0	0	0	0	1.9 × 2.5	1.1 × 0.6		
13	CMCC-CESM	rlilp1	0	0	0	0	3.4 × 3.8	2.0 × 1.6		
14	CMCC-CM	rlilp1	0	0	0	0	0.7 × 0.8	2.0 × 1.6		4.8
15	CMCC-CMS	rlilp1	0	0	0	0	3.7 × 3.7	2.0 × 1.6		5.1
16	CNRM-CM5	rlilp1	0	0	0	0	1.4 × 1.4	1.0 × 0.8	3.3	3.6
17	CNRM-CM5-2	rlilp1	0	0	0	0	1.4 × 1.4	1.0 × 0.8		
18	CSIRO-Mk3-6-0	rlilp1	0	0	0	0	1.9 × 1.9	1.9 × 1.9	4.1	4.8
19	FIO-ESM	rlilp1	0	0	0	0	2.8 × 2.8	1.1 × 0.6		
20	FGOALS-g2	rlilp1	0	0	0	0	2.8 × 2.8	1.0 × 1.0		
21	FGOALS-s2	rlilp1	0	0	0	0	1.7 × 2.8	1.0 × 1.0		
22	GFDL-CM2p1	rlilp1	0	0	0	0	2.5 × 2.0	1.0 × 1.0		
23	GFDL-CM3	rlilp1	0	0	0	0	2.0 × 2.5	1.0 × 0.9	4.0	4.6
24	GFDL-ESM-2G	rlilp1	0	0	0	0	2.0 × 2.0	1.0 × 0.9		2.8
25	GFDL-ESM-2M	rlilp1	0	0	0	0	2.0 × 2.5	1.0 × 0.9		3.6
26	GISS-E2-H	rlilp1	0	0	0	0	2.0 × 2.5	1.0 × 1.0		2.8
27	GISS-E2-H-CC	rlilp1	0	0	0	0	2.0 × 2.5	1.0 × 1.0		2.7
28	GISS-E2-R	rlilp1	0	0	0	0	2.0 × 2.5	1.0 × 1.3		2.7
29	GISS-E2-R-CC	rlilp1	0	0	0	0	2.0 × 2.5	1.0 × 1.3		2.6
30	HadCM3	rlilp1	0	0	0	0	3.7 × 2.5	1.2 × 1.2		
31	HadGEM2-AO	rlilp1	0	0	0	0	1.9 × 1.2	1.0 × 1.0		
32	HadGEM2-CC	rl/ 2ilp1	0	0	0	0	1.3 × 1.9	1.0 × 0.8		4.5
33	HadGEM2-ES	rl/ 2ilp1	0	0	0	0	1.3 × 1.9	1.0 × 0.8	4.6	4.8
34	INMCM4	rlilp1	0	0	0	0	1.5 × 2.0	0.7 × 0.4	2.1	3.3
35	IPSL-CM5A-LR	rlilp1	0	0	0	0	1.9 × 3.8	2.0 × 1.6	4.1	4.8
36	IPSL-CM5A-MR	rlilp1	0	0	0	0	1.3 × 2.5	2.0 × 1.6		5.1
37	IPSL-CM5B-LR	rlilp1	0	0	0	0	1.9 × 3.8	2.0 × 1.6		3.5
38	MIROC5	rlilp1	0	0	0	0	1.4 × 1.4	1.7 × 1.3	2.7	2.7
39	MIROC-ESM	rlilp1	0	0	0	0	2.8 × 2.8	1.4 × 0.8	4.7	4.0
40	MIROC-ESM-CHEM	rlilp1	0	0	0	0	2.8 × 2.8	1.4 × 0.8		4.1
41	MPI-ESM-LR	rlilp1	0	0	0	0	1.9 × 1.9	1.4 × 1.3	3.6	4.3
42	MPI-ESM-MR	rlilp1	0	0	0	0	1.9 × 1.9	0.5 × 0.4		4.2
43	MPI-ESM-P	rlilp1	0	0	0	0	1.9 × 1.9	1.5 × 1.5		
44	MRI-CGCM3	rlilp1	0	0	0	0	1.1 × 1.1	1.0 × 0.5	2.6	3.3
45	MRI-ESM	rlilp1	0	0	0	0	1.1 × 1.1	1.0 × 0.5		3.4
46	NorESM1-M	rlilp1	0	0	0	0	1.9 × 2.5	1.1 × 0.4	2.8	2.5
47	NorESM1-ME	rlilp1	0	0	0	0	1.9 × 2.5	1.1 × 0.4		2.6

For producing spatial analyses, model outputs were regridded to a common $1.5 \times 1.5^\circ$ lat/lon regular grid using conservative remapping. Evaluation was conducted over 1950–1999 or 1950–2005 (as marked) for ocean, climate driver, and teleconnection analyses, and for the IPCC AR6 baseline 1995–2014 for temperature and rainfall. Observed datasets used are the gridded Australian Water Availability Project (AWAP) temperature and rainfall for Australia (Jones et al., 2009; Raupach et al., 2009), HadISST1.1 for sea surface temperature (SST; Rayner et al., 2003), and Global Precipitation Climatology Project (GPCP) for Indo-Pacific rainfall (Adler et al., 2003).

Area average of mean annual temperature is given for the Australian land surface, area-average rainfall is reported four regions defined as “superclusters” (amalgamations of natural resource management regions) named Southern Australia, Eastern Australia, Northern Australia, and Rangelands covering the central area (see map in Figure 3e) in CSIRO and Bureau of Meteorology (2015).

2.2.1. Mean Climate

One way to evaluate climate models is to compare their simulation of the historical climate against observations (e.g., Flato et al., 2013). Doing so enables us to identify particular regions and processes where models may be in some way deficient (e.g., Christensen et al., 2013). This information may then be used to inform the confidence in the relevant climate change projections provided by these models. Here we evaluate the climatological mean state of the historical simulation of precipitation and SST, comparing the performance of a subset of CMIP5 and CMIP6 models for two seasons: June to November (JJASON) and December to May (DJFMAM). We focus this analysis on the region surrounding the Australian continent, including the two major ocean basins relevant to several large-scale circulations and climate drivers which influence the Australian climate: the Pacific and Indian Oceans (e.g., Risbey et al., 2009).

A common and long-standing mean-state bias in CMIP models over the years has been the “cold tongue bias,” which is the penetration of the equatorial Pacific cold tongue too far west (Li & Xie, 2014; Mechoso et al., 1995). This bias plays an important role in the simulation of current and future climate in the tropical Pacific and surrounding regions. For example, studies of CMIP5 models have shown that this bias can lead to a cold SST bias in the western Pacific which would contribute to a La Niña-like response to increasing greenhouse gases (Li et al., 2016; Ying et al., 2019). It also contributes to biases in the simulation of the El Niño Southern Oscillation (ENSO) and related teleconnections, leading to weakened Australian monsoon westerlies (Colman et al., 2011) as well as limited skill in the seasonal prediction of the Asian summer monsoon (Li et al., 2019). This bias affects the projections of regional rainfall in the western Pacific (e.g., Grose et al., 2014) and also the Northern Australian monsoon region (e.g., Brown et al., 2016).

Two methods are employed to evaluate the Pacific cold tongue bias adjacent to Australia. The first method is to use the eastern edge of the Indo-Pacific warm pool as a marker, defined as the equatorial longitude of the 28.5°C isotherm (Brown, Maes et al., 2013; Grose et al., 2014). In observations, this represents the boundary between the warm, fresh water of the warm pool and colder, saltier water of the cold tongue (Brown et al., 2013b; Grose et al., 2014) and is located at 186.5°E during the late historical period (JJASON, 1950–2005). This method, while useful, does have some drawbacks. In particular, the 28.5°C isotherm being the edge of the warm pool is true in observations, but this value may differ by up to 1° longitude in models (Brown et al., 2015). An alternative method is to introduce a cold tongue index (CTI), defined to be the bias in the SSTs averaged over the warm pool (155°E to 175°E , 10°S to 10°N). In this way, any extension of the models' cold tongue into the observed warm pool region would result in $\text{CTI} < 0$.

2.2.2. Extremes

Extremes indices, defined by the Expert Team on Climate Change Detection and Indices (ETCCDI) in Zhang et al. (2011), were calculated from daily precipitation, daily minimum temperature (tasmin), and daily maximum temperatures (tasmax) using the ClimPactv2 software (<https://climPact-sci.org/get-started/>) for both AWAP and models. These indices describe different aspects of precipitation and temperature extremes. We choose six of the possible 27 ETCCDI indices in order to measure aspects of intensity, frequency, and duration:

- TXx: annual maximum value of tasmax ($^\circ\text{C}$) (intensity)
- TNn: annual minimum value of tasmin ($^\circ\text{C}$) (intensity)
- wsdi (warm spell duration index): annual count of days with at least six consecutive days when tasmax: >90 th percentile (duration)

- Rx1day: annual maximum value of daily precipitation (mm) (intensity)
- R10mm: annual count of days when precipitation ≥ 10 mm (days) (frequency)
- CDD (maximum length of dry spell): maximum number of consecutive dry days (i.e., with precipitation < 1 mm) (days) (duration)

Fewer CMIP6 model outputs are available at the daily compared to the monthly scale, so only seven CMIP6 models were available to be analyzed (Table 1). Indices were calculated on the native grids of the observations and models before being interpolated onto the $1.5 \times 1.5^\circ$ lat/lon regular grid. Climatological values of the indices from 1995 to 2014 from AWAP are shown in Figure S1 in the supporting information.

Average recurrence intervals (ARI) quantify rare extremes used to assess damaging extremes (e.g., for building standards). ARI values of 1-, 5-, and 10-year values for daily precipitation and tasmax were calculated for the period 1950 to 1999, as well as for the period 2050 to 2099, enabling the projected change in ARI to be examined. While noting that there are various methods that can be used for calculating ARI values, the method used here is based on ranking the days in order of magnitude and then finding the day corresponding to the given ARI (i.e., the fifth highest daily value in the 50-year period is used for estimating the 10-year ARI, while the 50th highest value is used to estimate the 1-year ARI).

2.2.3. ENSO, IOD, and SAM

Special focus is given here to the simulation of the ENSO, the Indian Ocean Dipole (IOD) and the Southern Annular Mode (SAM), and their teleconnection to Australian rainfall, since these phenomena are important to Australian rainfall variability and may be important to future changes in the climate.

The ENSO and IOD exhibit teleconnections to winter-spring rainfall (JJASON) in Australia. ENSO variability is tracked using the Niño-3.4 index (Bellenger et al., 2014) and IOD using the Dipole Mode Index (DMI; Meyers et al., 2007; Liu et al., 2014). The DMI is defined as the difference of SST anomalies in the west equatorial Indian Ocean (50 to 70°E , 10°S to 10°N) minus those in the east (90 to 110°E , 10°S to 0°). Both indices had their seasonal cycles removed, and the resulting anomaly time series were detrended using a cubic polynomial fit. While the IOD is known to covary with ENSO (and vice versa), with the strongest impacts on rainfall over Eastern Australia (Cai et al., 2011; Meyers et al., 2007; Risbey et al., 2009), in this simple analysis, we do not separate the impacts of ENSO from the IOD.

Additionally, ENSO phase locking was examined over the period 1870–2014 in 13 CMIP6 models and 18 CMIP5 models for which SST data are available for both the historical and SSP585/RCP8.5 experiments for the full period and in HadISST. The Niño-3.4 index was calculated first by averaging full SSTs over the Niño-3.4 region (190°E to 240°E , 5°S to 5°N). The model Niño-3.4 indices show a pronounced long-term nonlinear trend, akin to a global warming signal. This nonlinear trend was estimated and removed by fitting a third-order polynomial function to the combined Historical and SSP5-85/RCP8.5 Niño-3.4 index.

The zonal structure of ENSO-related SST variability was evaluated using the standard deviation along the tropical equatorial Pacific (zonal average 2°S to 2°N) in observations (HadISST, 1870–2014) and CMIP simulations. All available historical experiments included 32 CMIP5 models and 28 CMIP6 models during the full period. An ensemble comparison of the historical experiments with available SSP5-85/RCP8.5 experiments was conducted based on a subset of 31 CMIP5 and 19 CMIP6 models for which both experiments were available.

The SAM is the leading mode of atmospheric variability in the Southern Hemisphere (Thompson & Wallace, 2000) and has also been shown to affect rainfall variability in Australia (Hendon et al., 2007). A positive phase of SAM refers to a poleward shift of the eddy-driven jet, resulting in increased rainfall over high latitudes and decreased rainfall over midlatitudes in all seasons, and also higher rainfall over the subtropics in austral spring-autumn (Hendon et al., 2014; Lim et al., 2016). We calculate the monthly SAM index following the definition of Gong and Wang (1999), as the difference in zonal mean sea level pressure anomalies between 40°S and 65°S in each CMIP model and compared with the observed SAM calculated from ERA-Interim reanalyses (Dee et al., 2011). The 1979–2005 time period is used for normalization in each case.

2.2.4. Marine Heatwaves

MHWs are periods of anomalously warm ocean temperatures, which can span several days to months (Hobday et al., 2016). In extreme cases, MHWs can have significant impacts on marine ecosystems, leading to loss of species and habitats (Smale et al., 2019). The frequency, duration, and intensity of MHWs have increased over the past century across the globe, and Australia's marine environment is no exception

(Oliver et al., 2018). Marine ecosystems are of vital importance to Australia's fisheries, aquaculture, tourism, and identity (Holbrook & Johnson, 2014; Johnson & Holbrook, 2014), and thus, the more extreme MHWs projected under climate change pose a significant risk. The representation of MHW intensities and durations in the historical period are evaluated in this paper.

MHW annual statistics were calculated from SST during 1982–2014 in CMIP6 and CMIP5 models (using historical and RCP8.5 simulations to match the available timespan of CMIP6 Historical) on a grid point basis and compared to the 0.25° lat/lon NOAA OI SST V2 product (Reynolds et al., 2007). Outputs were examined on native grids; then, nearest-neighbor interpolation was used to present data on the observed grid. MHW events were examined as events of SST over the 90th percentile of temperature on that calendar day (using an 11-day window centered on the given day in the 1996–2014 baseline in each model) for at least five consecutive days. MHW periods separated by less than 3 days are considered a single event. After computing the threshold for each calendar day, it was smoothed by applying a 31-day moving mean. The intensity of MHWs is thus taken as the maximum temperature anomaly of the event, relative to the climatological mean.

2.2.5. Dynamic Sea Level

In this study, we only consider the dynamic sea level (DSL) change simulated by the climate models. The other sea level components, including global ocean thermal expansion, land water storage change, and land ice loss from the glaciers and polar ice sheets, are not included here. The DSL is closely related to ocean density and circulation; thus, its regional distribution can be explained well by ocean dynamics. DSL change determines the regional pattern of change in sea level experienced at the coast. Observations and previous modeling suggest that there is considerable variation in DSL change around Australia in the past and the projected future, with higher rates of change in the north and east and lower rates on the south coast. Downscaling of CMIP5 sea level projections suggests these regional patterns could be enhanced compared to the global simulations (Zhang et al., 2017). Here we evaluate the simulation of DSL in 23 CMIP6 models and 30 CMIP5 models, examine their projections, and compare their projections to previous downscaled projections.

3. Evaluation

To inform confidence in future climate projections, we first evaluate some of the key features of climate model simulations. The Indian Ocean to the northwest and the Pacific Ocean to the northeast of Australia are both critical to Australian climate variability and change, both in terms of their mean state (e.g., relative temperature of Indian compared to Pacific) and also climate variability through processes including ENSO and IOD. Therefore, the focus here is on the entire Indo-Pacific region rather than just Australia.

3.1. Mean Climate

The bias in SST is similar between CMIP5 and CMIP6 (Figure 1), but with some locations where the bias is different in magnitude and some new features exist. The cool bias in JJASON in the Tasman Sea, Pacific Ocean, Inter-Tropical Convergence Zone (ITCZ), and the South Pacific Convergence Zone (SPCZ) regions is similar to CMIP5 in extent but slightly smaller in magnitude. There is a warm bias in the equatorial Indian Ocean during DJFMAM that was not present in CMIP5.

In observations, the equatorial 28.5 °C isotherm is located at 186.5°E. Most of the CMIP5 models simulate the 28.5 °C isotherm too far west, with the equatorial isotherm of the multimodel mean (MMM) located at 163.5°E. In CMIP6, there is a marked reduction of this bias, with the MMM isotherm at 172.5°E (Figure 2). Figure 2d shows the model spread of the longitude of the 28.5 °C isotherm, with more than 81% of CMIP5 and 93% of CMIP6 models simulating the isotherm too far west. Note that although a larger fraction of CMIP6 models place the equatorial isotherm too far west, the interquartile range is smaller and closer to the observed value. Using the CTI (defined in section 2.2) as an alternative measure of the cold tongue bias, the spread of the CTI in the models is quantified in Figure 2e, with the CMIP5 MMM being -0.39 °C and the CMIP6 MMM being -0.12 °C. We find 79% and 67% of CMIP5 and CMIP6 models, respectively, have a CTI < 0. Both methods presented here show that there is an encouraging improvement in the cold tongue bias in the CMIP6 models. It is expected that this improvement will lead to a reduction in the related biases discussed previously.

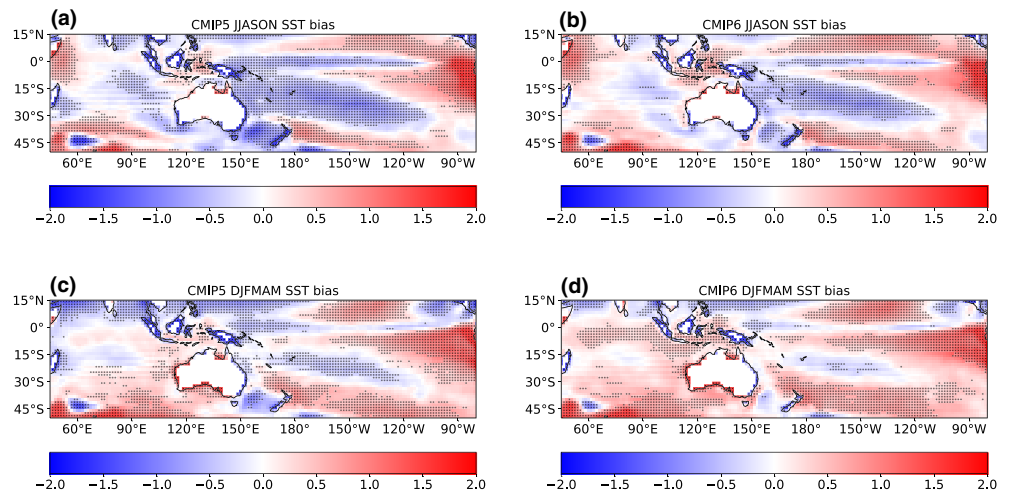


Figure 1. Multimodel sea surface temperature bias (°C) for CMIP5 (left) and CMIP6 (right) models, shown for June to November (JJASON, top) and December to May (DJFMAM, bottom) averages. Biases are calculated against the HadISST observation-based dataset for the period 1995–2014. Stipples represent locations where greater than two thirds of models agree on the sign of the bias.

Like temperature, the spatial distribution of biases in seasonal precipitation is similar in the two ensembles (Figure 3), including a wet bias in the cold tongue region and Maritime Continent persisting in CMIP6. A dry bias in the southeast SPCZ region and wet bias in the off-equatorial east Pacific indicate a continued double-ITCZ or overly zonal SPCZ bias in CMIP5. This has not changed substantially in CMIP6. The dry bias in the eastern Indian Ocean during JJASON is increased for CMIP6 models surveyed. There was an overly zonal SPCZ in CMIP5 (Brown, Moise, et al., 2013) that remains in CMIP6. Excessive precipitation biases remain in the Maritime Continent region, which may relate to local Hadley circulation biases (e.g., Toh et al., 2018). The improvement in the cold tongue bias in CMIP6 models over the western equatorial Pacific (Figure 2) occurs over a region that was associated with projected drying over Northern Australia in CMIP5 models (Brown et al., 2016). Looking at proportional (%) rainfall in more detail over Australia compared to the gridded AWAP rainfall dataset (Figures 3e and 3f), we see a mean wet bias in most locations, but with dry biases related to topography and coastlines, as expected from the GCM coarse resolution. The large positive proportional (%) biases are in areas of very low seasonal rainfall.

Overall, the pattern correlation of precipitation and temperature climatologies is improved in CMIP6 compared to CMIP5 (Figures 4a and 4c). The root-mean-squared (RMS) error when comparing model climatologies to observations is lower for the CMIP6 ensemble compared to CMIP5, although the improvement is less pronounced for surface temperature than for precipitation (Figures 4b and 4d).

3.2. Extremes

The evaluation of extremes based on the current CMIP6 model sample should be interpreted with caution as there are fewer CMIP6 than CMIP5 models (seven models compared to 29, see Tables 1 and 2). This means the reduction in spread of CMIP6 compared to CMIP5 is at least partly due to a smaller number of models in the ensemble (Figure S2). Bearing this in mind, we draw the following conclusions.

For all indices analyzed, observed values sit within the spread of both CMIP5 and CMIP6 (Figure S2) and for hottest day of the year (TXx), count of days with more than 10 mm of rainfall (R10mm), and maximum length of dry spell (CDD), observations sit close to the MMM (although, not surprisingly, have more inter-annual variability). However, the coldest night of the year (TNn) is generally cooler in observations than the MMM of either CMIP5 or CMIP6, and there are fewer warm spells (wsdi). In addition, the wettest day of the year (Rx1day) is about 5 to 10 mm more intense in CMIP6 compared to CMIP5 and closer to the AWAP observations. Broadly speaking, minimum temperature extremes (e.g., TNn) seem to be warmer

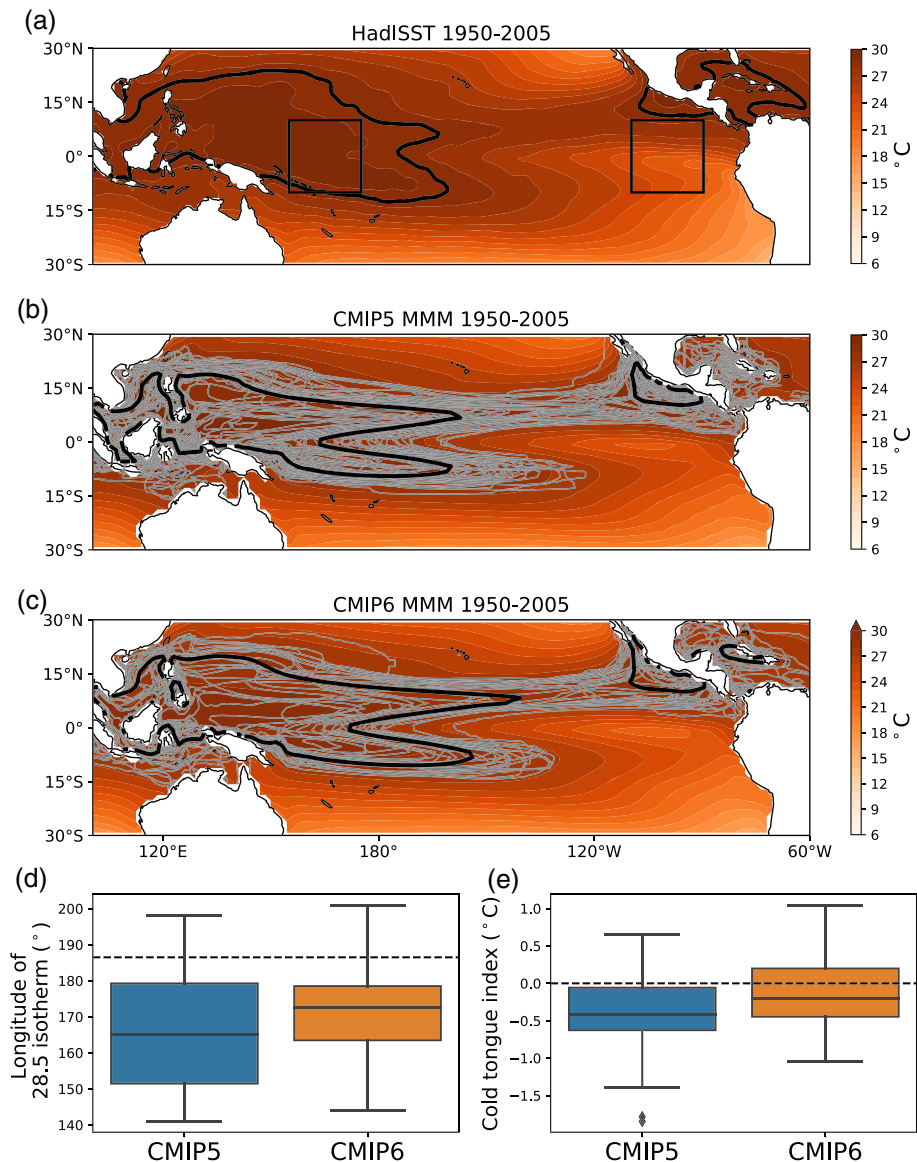


Figure 2. Climatological SSTs from 1950 to 2005 for JJASON. Top panel shows HadISST1.1, where the thick black line shows the 28.5 °C isotherm and the box shows the location of the CTI region. The other two maps show the CMIP5 and CMIP6 MMM climatological SSTs for the same period, where thin gray lines show the location of the 28.5 °C isotherm for each individual model, and the thick black line shows the MMM. Box plots at the bottom show the equatorial longitude of the 28.5 °C isotherm (left) and the CTI (right) for CMIP5 (blue) and CMIP6 (orange). In these boxplots, the horizontal dashed line shows the observed longitude of the 28.5 °C isotherm, boxes encompass the interquartile range (25–75% of the model spread), whiskers encompass models which lie within 1.5 times the interquartile range of the box borders, outliers are marked as diamonds, and the horizontal line in the boxes shows the median.

and maximum temperature extremes (e.g., TXx) seem to be cooler in CMIP6 compared to CMIP5, at least based on the currently available models. In addition, the spread is much smaller in CMIP6 compared to CMIP5 so there are fewer models with very low or very high values across the majority of indices. One exception is Rx1day where the upper extremes are larger in CMIP6.

Mean biases in extreme indices in the model ensembles compared to AWAP are very similar in terms of spatial pattern and magnitude, although in CMIP6, we see some reduction of the bias in TNn and Rx1day over Northern and Eastern Australia (Figure S3).

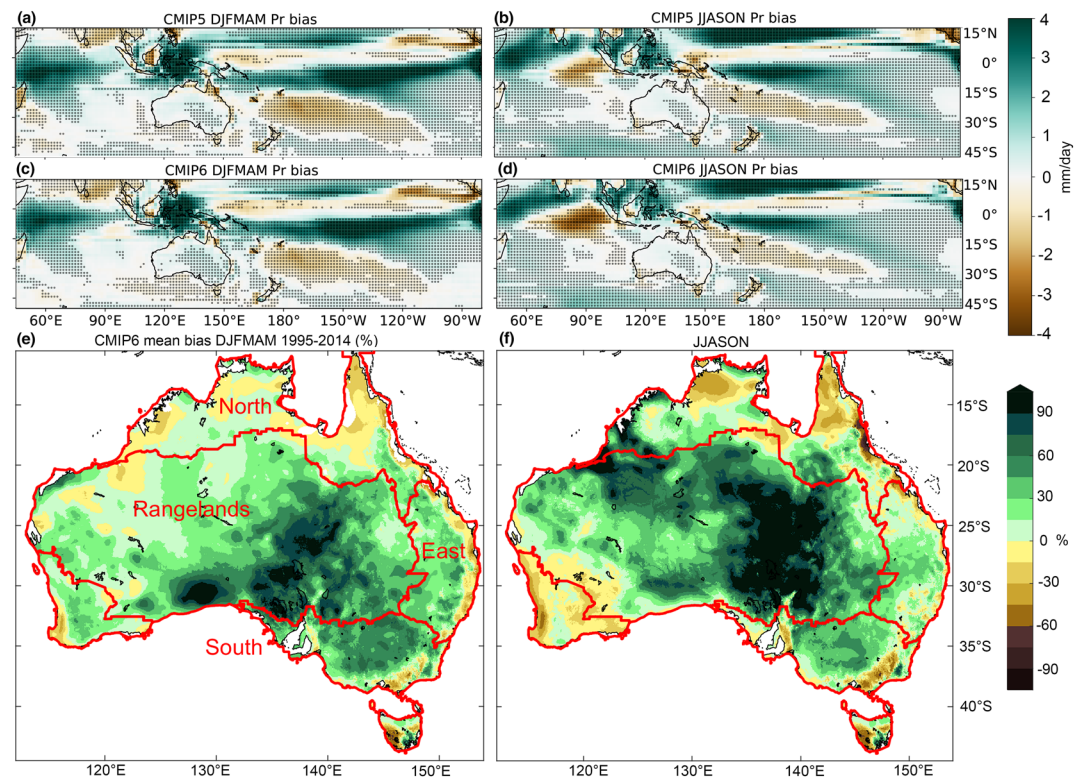


Figure 3. Precipitation bias in CMIP5 and CMIP6 for DJFMAM and JJASON. Upper four panels (a–d) show MMM bias compared to GPCP observations (mm day^{-1}); stipples represent locations where greater than two thirds of models agree on the sign of the bias. Lower two panels show MMM CMIP6 precipitation bias over Australia over 1995–2014 compared to AWAP (%); red lines indicate the borders of the four “supercluster” averaging regions: Northern Australia (North), Rangelands, Southern Australia (South), Eastern Australia (East).

In summary, compared to observations, the results for CMIP5 and CMIP6 are similar for temperature and precipitation extremes, although with some indication that CMIP6 has reduced some of the warm bias in TNn and dry bias in Rx1day. This could change as more CMIP6 models become available.

3.3. ENSO, IOD, and SAM

First, we assess the simulation of some important features of ENSO, IOD, and SAM and then examine the teleconnection of ENSO and IOD to Australian rainfall. Seasonal phase locking of ENSO is similar in CMIP5 and CMIP6 (Figure S4). In observations, the annual maximum and minimum ENSO variability is found in in December and June, respectively. The CMIP5 and CMIP6 MMM ENSO variability is similar to observations, with the extreme values occurring in December and June. While the simulated seasonal phase locking is realistic, the ENSO events simulated by the CMIP6 models are stronger than those in observations all year round. The MMM intensity of ENSO events is more realistic in the CMIP5 Historical experiments (dashed blue curve); however, the seasonal phase locking is not as realistic with a smaller annual variation in ENSO variability.

The zonal structure of SST variability represented by the interannual standard deviation is improved in CMIP6 compared to CMIP5 (Figure S4, bottom panel). In the observations, the strongest interannual variability occurs in the eastern tropical Pacific close to the 100°W longitude. The majority of CMIP5 and CMIP6 models show this peak variability eastwards of 130°W with a few exceptions (CSIRO-Mk3-6-0 and INM-CM4-8). Many of the models in both CMIP5 and CMIP6 simulate stronger variability in the historical period than observed, in particular in the central and western Pacific and in the eastern Pacific (the MMM of CMIP6 is in fact higher than CMIP5). However, the location and intensity of simulated interannual variability varies among the models and from the observed and is mostly overestimated in the central and western Pacific.

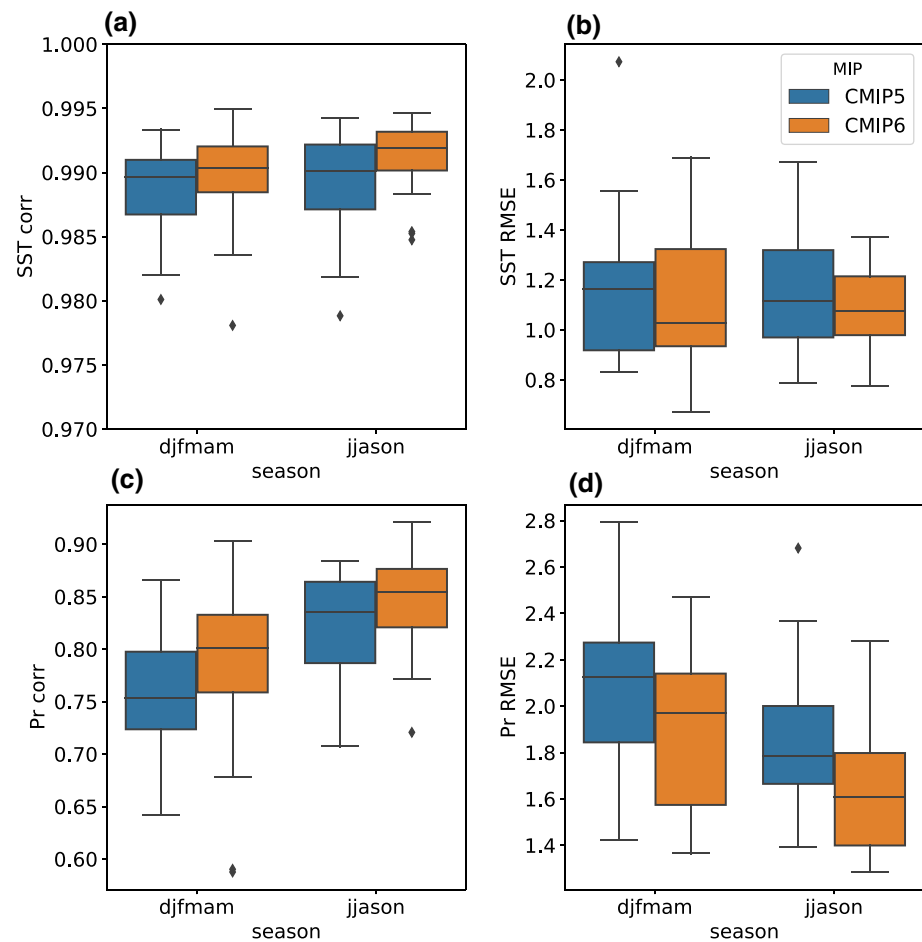


Figure 4. Boxplots of spatial correlation (left) and RMSE (right) of the 1996–2014 climatologies for modeled precipitation compared to GPCP (top) and modeled sea surface temperature compared to HadISST (bottom), separated by seasons DJFMAM and JJASON, as well as by Inter-comparison Project (CMIP5 in blue and CMIP6 in orange). Metrics are calculated for the region 45 to 280°E, 10°N to 50°S.

The observed positive trend in SAM, stronger in austral summer, in recent decades (1979–2005) is reproduced in the MMM of both CMIP5 and CMIP6, with some bias in the seasonal signature. In particular, models show an underestimation of trends in summer and winter and overestimation in spring. Both ensembles have a large model spread but with a narrower spread in summer in CMIP6 compared to CMIP5 (Figure S5). Otherwise, results are similar between CMIP5 and CMIP6 (Figure S5). Projections of SAM (Figures S5b and S5d) are found in a later section.

The strongest observed correlation of ENSO and rainfall is in Eastern Australia (Figure 5a), whereas the strongest correlation with IOD is in Southern Australia (Figure 5b). It is notable that the IOD and ENSO teleconnections are remarkably well separated during winter-spring over the Australian mainland except for the monsoonal north and the Murray-Darling Basin. Much of the IOD teleconnection with rainfall in the central and western Murray-Darling Basin (and part of the monsoonal north) is due to ENSO (Risbey et al., 2009). ENSO teleconnections to Northern and Eastern Australia tend to be stronger than IOD teleconnections to these regions, while the reverse is true for Southern Australia and the Rangelands.

The simulation of the rainfall teleconnection of ENSO and IOD in CMIP5 and CMIP6 over the Northern and Eastern Australia superclusters is shown in Figures 5c and 5d, and IOD teleconnections to Southern Australia and the Rangelands superclusters are shown in Figures 5e and 5f. The strength of the ENSO and IOD teleconnection to each region's rainfall is well correlated with the associated amplitude of Niño-3.4 and DMI. This strong relationship was found in CMIP3 models, although CMIP5 models generate reduced spread in Niño-3.4 and DMI amplitudes than CMIP3 (Cai et al., 2009; Cai & Cowan, 2013). The

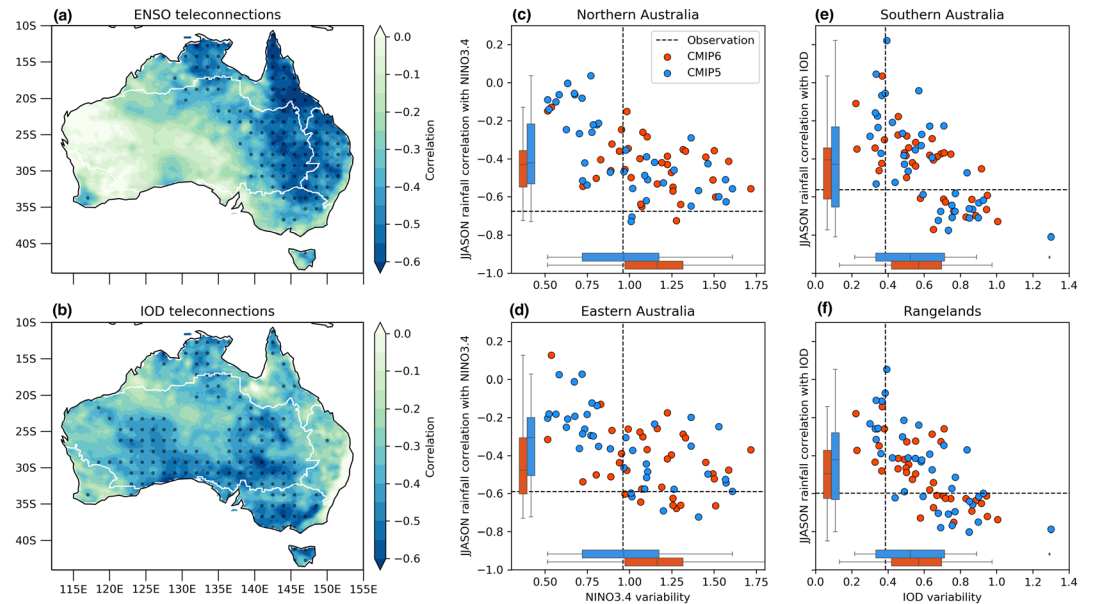


Figure 5. Indo-Pacific teleconnections to Australian rainfall. The maps show observed correlation coefficients between AWAP winter-spring rainfall and SST indices representing the El Niño Southern Oscillation (a; Niño-3.4) and the Indian Ocean Dipole (b, DMI) in JJASON, where stippling indicates the 99% significance of the p value. Scatter plots show the correlation coefficient of the rainfall averaged over each of the four “supercluster” (y axis, borders of regions shown in map plots) with the standard deviation of each index Niño-3.4 or DMI (x axis) in: Northern Australia (c), Eastern Australia (d), Southern Australia (e), and Rangelands (f). Values for observations (dashed lines), CMIP6 models (orange circles), and CMIP5 models (blue circles) are shown. The boxplots within each scatterplot show the interquartile model ranges of the x and y axis variables for the CMIP5 (blue) and CMIP6 (orange) models; the whiskers show the rest of the distribution, except for points that are determined to be “outliers.”

trend towards less diversity in ENSO amplitudes from CMIP3 to CMIP5 (Bellenger et al., 2014) appears to continue from CMIP5 to CMIP6 (horizontal boxplots, Figures 5c–5f).

For Northern and Eastern Australia, CMIP5 and CMIP6 models underestimate the strength of the teleconnection relative to ENSO (the vertical boxplots sit well above the horizontal line marking the observation, Figures 5c and 5d). For Southern Australia and the Rangelands regions which are evaluated for their teleconnection to the IOD, the strength of the teleconnection is still weak but better represented (the vertical boxplots sit just above the horizontal line representing the observations; Figures 5e and 5f). The teleconnection is weak in both CMIP generations despite the fact that the simulated IOD variability is much stronger than observed (the horizontal boxplots lie to the right of vertical line showing the observed IOD amplitude, Figure 5c and 5f). The overly strong IOD amplitudes are likely due to model mean-state biases with respect to the climatological zonal gradient of the equatorial Indian Ocean thermocline, which in turn generate biases in the mean easterlies and SST gradient (Cai & Cowan, 2013).

CMIP6 models show either an improvement or little change in simulating the ENSO and IOD winter-spring rainfall teleconnection over the Australian mainland. The newest generation of models outperform CMIP5 in terms of the strength of their ENSO teleconnections to Northern and Eastern Australia, as demonstrated by the smaller size of vertical box plots (and whiskers; in Figure 5), meaning there is fewer outlier models compared to CMIP5. Yet ENSO variability in CMIP6 models is both unrealistically large and larger than that in CMIP5 models, as shown by the shift in the horizontal box plots in Figure 5 to the right. In CMIP5, there is a tendency for models with a stronger ENSO amplitude to generate stronger IOD variability (Liu et al., 2014); however, the overly large ENSO amplitudes in CMIP6 do not appear to translate into stronger IOD amplitudes.

3.4. Marine Heatwaves

Modeled MHWs tend to persist longer, are more spatially extensive, and less intense than observed events, primarily due to the model coarse spatial resolutions (Frölicher et al., 2018; Pilo et al., 2019). Thus, with

higher atmospheric and oceanic spatial resolutions in the CMIP6 models (c.f. Table 1), there is some hope for improved simulation of mesoscale processes that drive extreme events. In this analysis, we examine whether the representation of MHWs has improved in CMIP6 relative to CMIP5 (Oliver et al., 2019; their Supplementary Figure 1). We evaluate MMM representations of MHW intensities and durations in SST data. The MHW statistics are computed on native model grids, to avoid smoothing of small-scale features that may be removed during regridding. Only in the final instance are model results regridged using nearest-neighbor interpolation (see section 2.2).

The mean annual maximum MHW intensities are shown for HadISST, CMIP5 MMM, and CMIP6 MMM over the period 1982–2014 (Figures 6a–6c). MHW intensity is measured as the maximum excursion from the seasonally varying climatology ($^{\circ}\text{C}$), on a single day in a given year. The day of maximum intensity is further constrained to occur within a MHW event—a period of at least 5 days of extreme warmth (see section 2.2 for further details). The strongest MHW intensities tend to occur off the southeast coast of Australia in observations (Figure 6a). The MMMs show a similar hotspot (Figures 6b and 6c) but shifted farther south. The differences between the MMMs and observed data (Figures 6d and 6e) show that models generally underestimate MHW intensity. However, encouragingly, the biases appear to be weaker in the CMIP6 model mean. The time series of area-average MHW intensities further highlight the typically higher values in

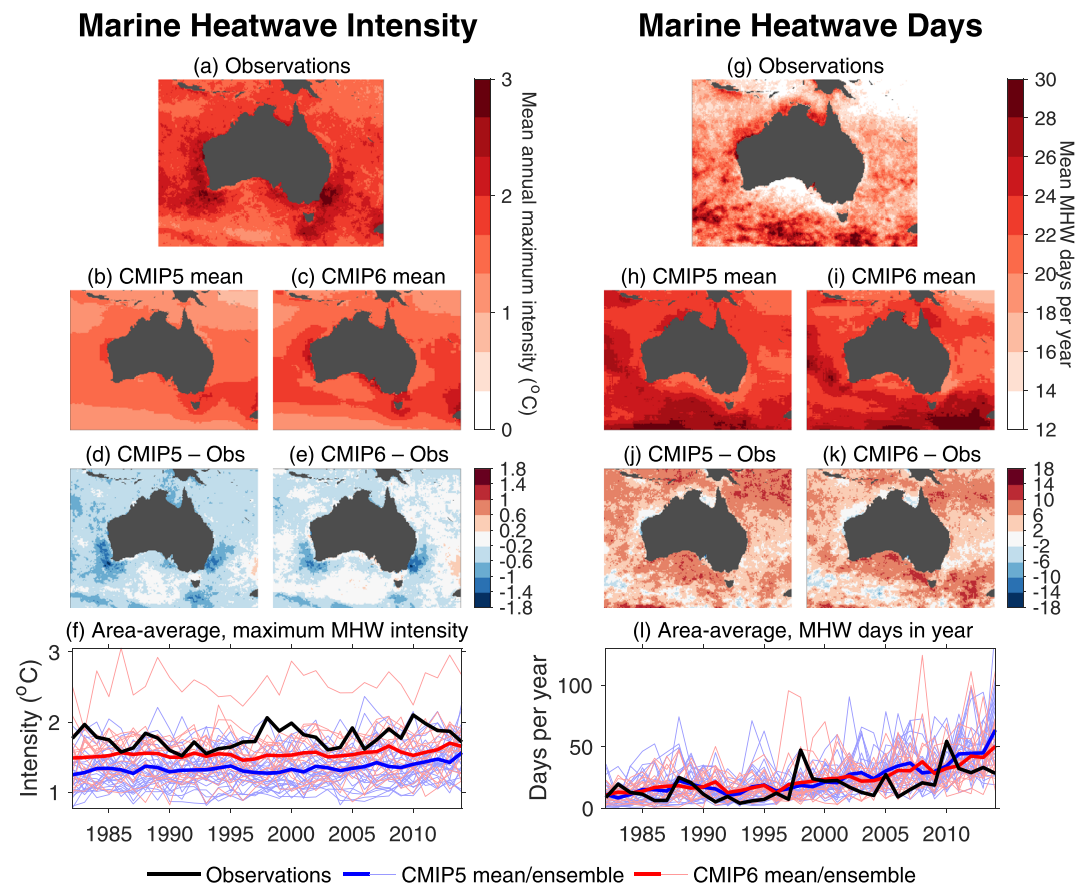


Figure 6. Marine heatwave (MHW) characteristics in observations, CMIP5, and CMIP6 over the period 1982–2014 around Australia. Left panels show annual maximum MHW intensity relative to the climatology of the baseline period of 1996–2014, which is first computed for each calendar year, and each grid point (see section 2.2). (a–c) Observed time-mean of the annual maximum MHW intensity, (d–e) the MMM difference between CMIP5/6 and observed time-mean, (f) annual time series of the area average of maximum MHW intensity over the region depicted in (a–e) for the observations, individual CMIP5 and CMIP6 model realizations (feint lines), and the model means (dark lines). Right panels show the number of MHW days per year. (g–i) time-mean of the number of MHW days occurring each year, (j–k) the MMM difference between CMIP5/6 and observed time-mean, and (l) as in (f), but for the annual MHW days.

CMIP6 as compared with CMIP5 (Figure 6f). One of the CMIP6 models, the *NESM3* model, exhibits significantly larger MHW intensities than any other model or observations. *NESM3* simulates particularly strong variability of SST during the summer season, and thus, the anomalous SSTs during MHWs in the summer are large. Omitting this single model does not noticeably alter the CMIP6 model mean.

The mean number of annual MHW days tends to be overestimated in both CMIP5 and CMIP6 MMMs (Figures 6g–6k). There appears to be a slight improvement of this bias in CMIP6 (c.f. Figure 6j), but the improvement is less clear than for MHW intensity.

This initial assessment suggests that CMIP6 simulates MHWs closer to observations than CMIP5, but more models are necessary to determine whether or not the improvement from CMIP5 is significant. Although the MHW intensities look to be much improved, the means of the CMIP5 and CMIP6 model intensities are not significantly different (at the 95% level under a two-sample Student's *t* test), nor are the distributions of intensities (at the 95% level under a two-sample Kolmogorov–Smirnov test). There is also no statistically significant intermodel correlation between mean spatial grid size in the Australian marine region and mean MHW intensity nor mean annual MHW days.

3.5. Dynamic Sea Level

The observed mean sea level over 1992–2012 (Maximenko et al., 2009) shows the effect of ocean currents, as the upper ocean circulation approximately follows contours of constant sea level (Figure 7a). For example, the subtropical ocean gyre can be easily recognized in the midlatitude South Pacific Ocean, with sharper sea level gradient near the east coast of Australia in the East Australian Current (EAC) region than in the interior of South Pacific. Compared with the observations, both the CMIP5 and CMIP6 ensembles show

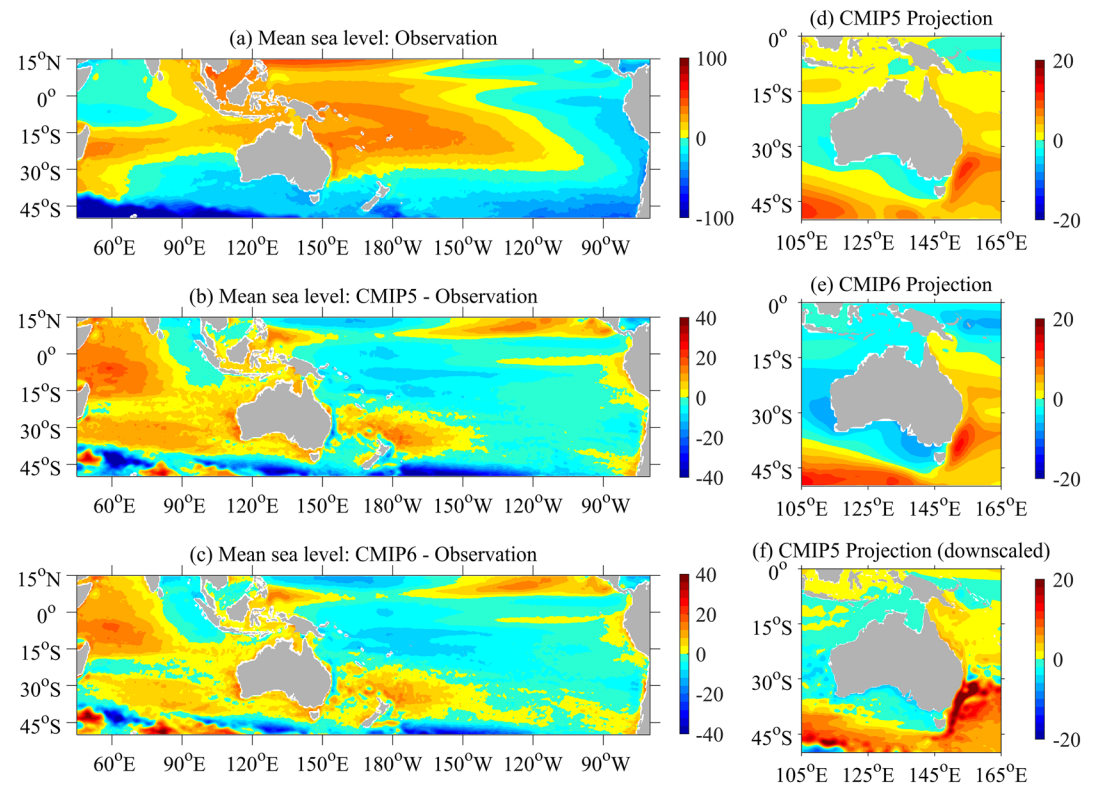


Figure 7. Mean sea level (cm) and dynamic sea level projections (cm). (a) Observed mean sea level (Maximenko et al., 2009), (b) the CMIP5 MMM difference relative to observed mean sea level, and (c) CMIP6 MMM difference. Regional means over the figure domain (50 to 290°E, 50°S to 15°N) have been removed from both CMIP5/6 ensembles and observations before calculating the differences in (b) and (c). Right panels show dynamic sea level projections due to ocean density and circulation change for the Australian region over 2080–2099 relative to 1995–2014 from (d) the CMIP5 ensemble under RCP8.5, (e) CMIP6 ensemble under SSP5-8.5, and (f) dynamically downscaled CMIP5 ensemble under RCP8.5.

considerable mean sea level biases around Australia which have been slightly reduced from CMIP5 to CMIP6 (Figures 7b and 7c), as indicated by a smaller RMS error between CMIP5/6 ensemble and observations (5.5 cm for CMIP5 and 4.4 cm for CMIP6) over the region closely surrounding Australia (105 to 150° E, 0 to 45°S). The relatively low (high) sea level biases in the western (eastern) tropical Pacific exist in both CMIP5 and CMIP6. Such bias pattern could be explained by the weaker simulated trade winds in the central Tropical Pacific relative to the observations (Lee et al., 2013) and may be closely related to the cold tongue biases seen in the SST field (Figures 1 and 2). Projection of DSL (Figures 7d–7f) is discussed in a later section.

4. Projections

4.1. Mean Annual Temperature

Under SSP5-85, we see that the upper range of CMIP6 projections by 2100 is hotter than CMIP5 under RCP8.5 for Australia and for the globe (Figure 8a). The value of projected temperature change between the AR6 baseline 1995–2014 and the end of century period 2080–2099 in CMIP6 (Table 1, panels to the right in Figure 8a) includes a group of models with a temperature projection higher than any CMIP5 model with values above 5.5 °C Australia. As more models are added, the apparent gap between this group of models and the rest may be filled. There are differences in the composition of greenhouse gases and aerosol forcings between RCP8.5 and SSP5-85; however, both reach 8.5 W m⁻² enhanced radiative forcing by 2100 so the difference in the forcing scenarios is unlikely to explain much of the difference in temperature change between the two ensembles.

Using the methods of Schurer et al. (2017) to account for warming from preindustrial to the AR5 baseline, we see that these warmer projections suggest that the global warming target of 2 °C since the preindustrial era specified in the Paris agreement is likely to be met sooner using the CMIP6 ensemble as a guide (Figure 8b). As more models are added the CMIP6 curve will change slightly, but the earliest crossing from the hottest models will certainly remain.

Australian warming for the period 2080–2099 under SSP5-85/RCP8.5 is less enhanced relative to global warming in the current CMIP6 models than in CMIP5 (Figure 8c), with no model producing a ratio of Australian to global warming greater than 1.1, whereas CMIP5 contains 18 out of 35 models with ratios over 1.1 with values up to 1.4. This may be due in part to the greater warming of the Pacific and Northern Hemisphere continents at this timeframe in CMIP6, raising the global value relative to the Australian value (Figures 8d and 8e). The basic patterns of warming remain, such as enhanced warming over the Arctic, greater warming over land than ocean, and delayed warming in the Southern Ocean and the north Atlantic; however, the relative magnitudes of these are different in the two ensembles. While the temperature projection is generally higher, the projected change in the north Atlantic and Southern Ocean are lower than in CMIP5, suggesting larger ocean heat uptake and that the slowdown in Atlantic meridional overturning circulation is in fact stronger (Figure S6).

The effect of higher climate sensitivity on the projected change is seen in these results for the end of the century where the signal is strongest but is less apparent for near-term periods. Under the highest emissions scenario (SSP5-85), and using the AR5 baseline of 1986–2005 and the 10th–90th percentile of the model range for direct comparison with the existing Australian national projections (CSIRO and Bureau of Meteorology, 2015), we see the range of change is not significantly different to 2020–2039 (0.7 to 1.4 °C in both) or by 2040–2059 (1.4 to 2.4 °C in CMIP5, 1.6 to 2.8 °C in CMIP6). After midcentury, the two ensembles are significantly different (using a two-tailed Student's *t* test) under SSP5-85/RCP8.5, especially at the top end, for both 2060–2079 (2.2 to 3.7 °C in CMIP5, 2.1 to 4.6 °C in CMIP6) and 2080–2099 (2.8 to 5.1 °C in CMIP5, 3.5 to 6.5 °C in CMIP6). The timing of the temperature rise appears to be consistent with a previous finding that while there is a group of models with high ECS, their transient climate response (TCR) measure of climate sensitivity, defined as the global mean temperature change for a doubling of CO₂ in a 1% per year increasing CO₂ experiment, appears to have not increased by as large a margin as the ECS. The different change to TCR compared to ECS suggested that high sensitivity is expressed as higher temperatures mainly at longer timescales. Using the 1850–1900 baseline as an approximation for the preindustrial climate, some models within CMIP6 project changes in global and Australian temperature of over 7 °C before the end of the century, which is unprecedented in CMIP5.

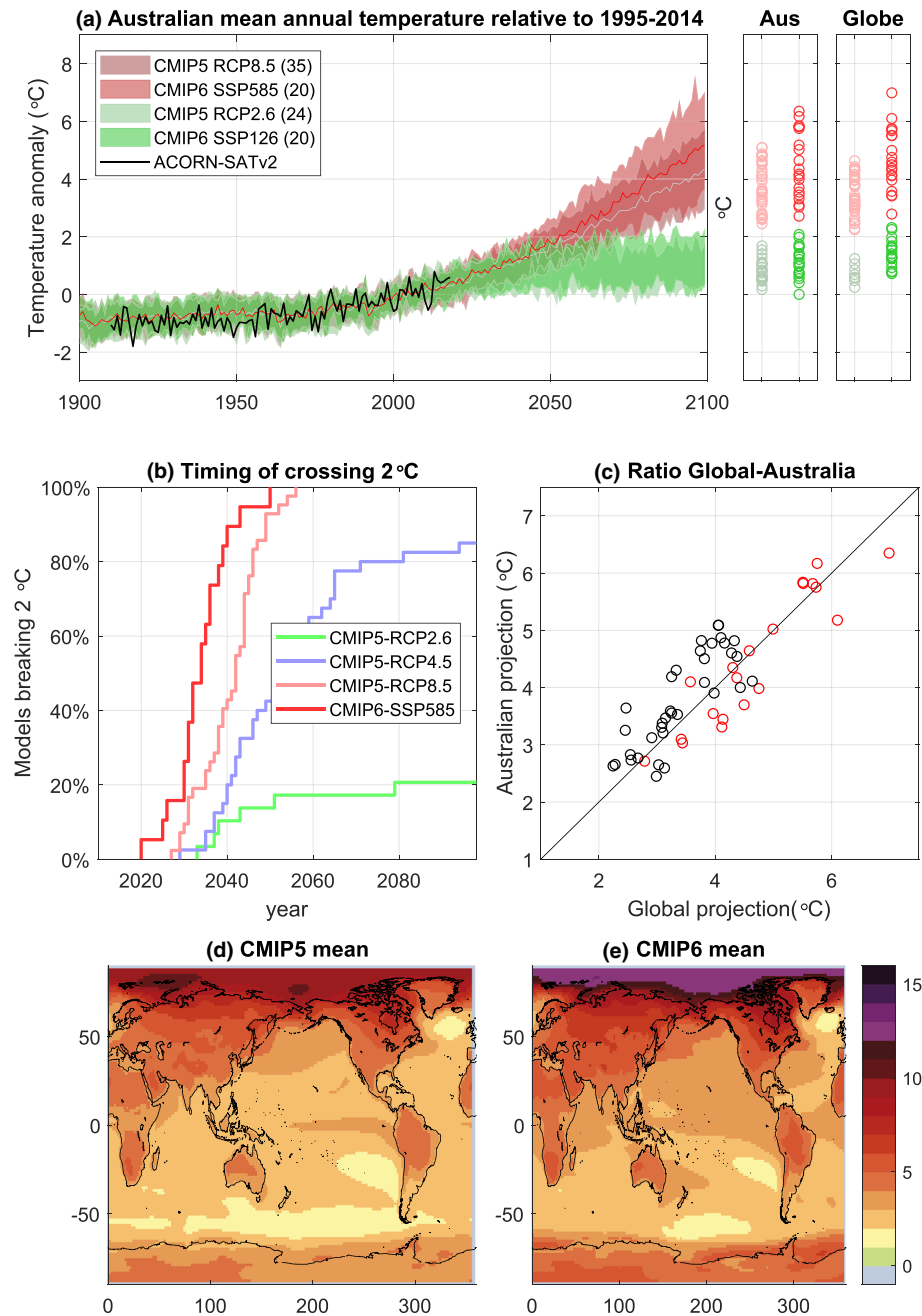


Figure 8. Mean annual surface air temperature in observations, CMIP5 and CMIP6. (a) Australian mean temperature anomaly from the 1995–2014 mean showing 10–90 percentile of model range and the MMM for RCP8.5 in CMIP5 (light red band, gray line), SSP5-85 in CMIP6 (red band, red line), RCP2.6 in CMIP5 (light green band), SSP1-26 in CMIP6 (green band), panels to the right show the value for individual models in 2080–2099 (CMIP5 on the left, CMIP6 on the right); (b) timing of when model simulations cross 2 °C global warming since preindustrial times calibrated to the 1986–2005 period (methods taken from Schurer et al., 2017); (c) ratio of global to Australian warming at 2080–2099 (red is CMIP6, black is CMIP5); (d) multimodel mean warming between 1995–2014 and 2080–2099 in CMIP5, and (e) as for (d) but in CMIP6.

The higher projection for Australia is expected from the higher ECS values in some models and is in fact quantitatively in line with the ECS values. Grose et al. (2016) scaled CMIP5 projections by ECS values to estimate Australian temperature projections under the full *likely* range of ECS, and if ECS is 6 °C, then we may expect a projection of 5.4 to 6.7 °C (using AR5 baseline of 1986–2005 to 2080–2099) with linear scaling and

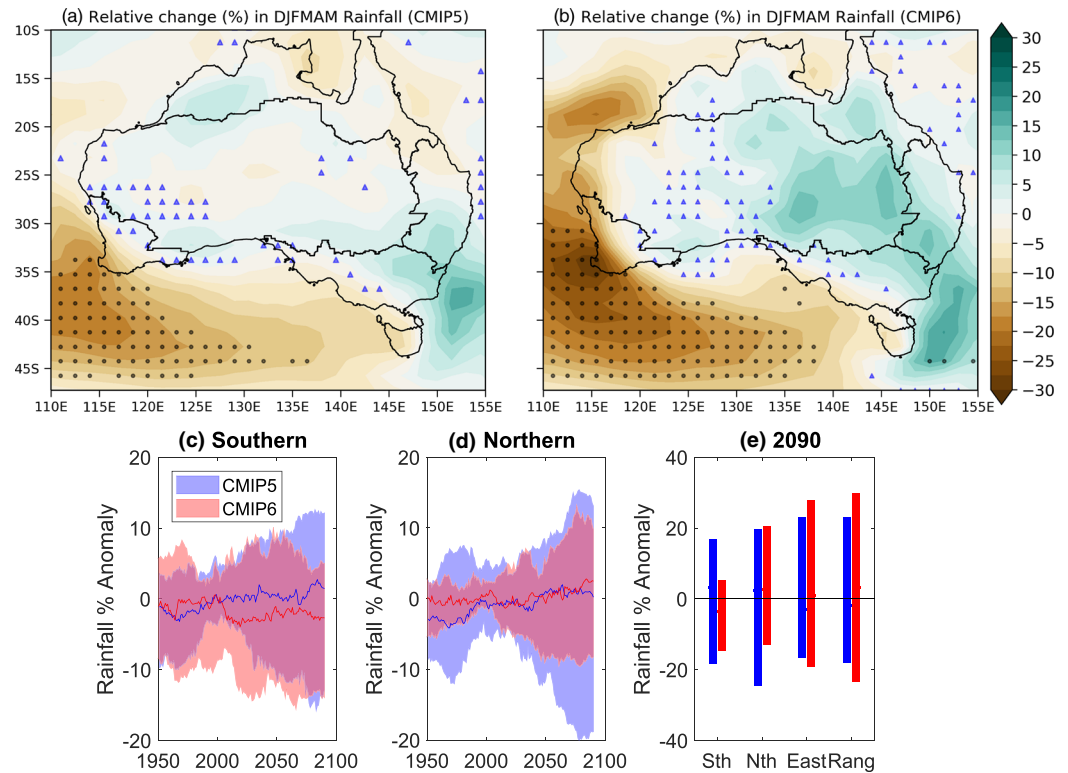


Figure 9. Rainfall projection (%) for DJFMAM for 1995–2014 to 2080–2099 under high emissions (RCP8.5 and SSP5-85). (a) CMIP5 multimodel mean (MMM), stippling shows >90% model agreement on sign of change, and blue triangles show regions of small change where the MMM change is less than 0.2 times the MMM standard deviation, and less than 20% of models show magnitude of change greater than 2 times the model standard deviation; (b) CMIP6 MMM; (c) time series of the 10–90% range and median of 20-year running mean of CMIP5 and CMIP6 averaged over the Southern region (blue for CMIP5, red for CMIP6, violet in areas where they overlap); (d) as for (c) but the northern region; and (e) range of change in 2080–2099 for each of the four regions (10–90% range, median).

6.0 to 8.5 °C using proportional scaling. The new results with ECS values over 5 °C give projections from this baseline of 6.1 to 6.6 °C, suggesting that the scaled results were broadly indicative.

There are different rates of 20-year warming in the two ensembles from around midcentury for both the globe and Australia, with rates of warming for Australia exceeding 0.8 °C/decade in some models (Figure S6). There are also some different 20-year trends in earlier periods, especially at the global scale that are likely related to different historical forcing and different model responses to this forcing in CMIP6 and need further investigation.

4.2. Rainfall

Projected change in rainfall during austral summer and autumn (DJFMAM) is broadly similar in CMIP5 and CMIP6 (Figure 9), with a few notable differences. Unlike CMIP5, the range of change from these 16 CMIP6 models does not include models with a large decrease in rainfall in Northern Australia (Figure 9d). In austral winter and spring (JJASON), CMIP6 supports the broad pattern of rainfall change produced in CMIP5, with greater model agreement (so far) for rainfall to increase in western Tasmania and decrease down the entire eastern seaboard (Figure 10). There are two cases where the projection may be more constrained than CMIP5 based on the existing model sample: Southern rainfall in JJASON and Northern rainfall in DJFMAM. There are other cases where the range already appears wider than CMIP5 at either end of the distribution (or both): notably in Rangelands and Eastern Australia. Projections for 3-month seasons (DJF, MAM, JJA, and SON, Figure S7) show a further breakdown of the seasonal signature in rainfall change and feature broader areas of model agreement on little change in summer and autumn than is seen in DJFMAM as a whole.

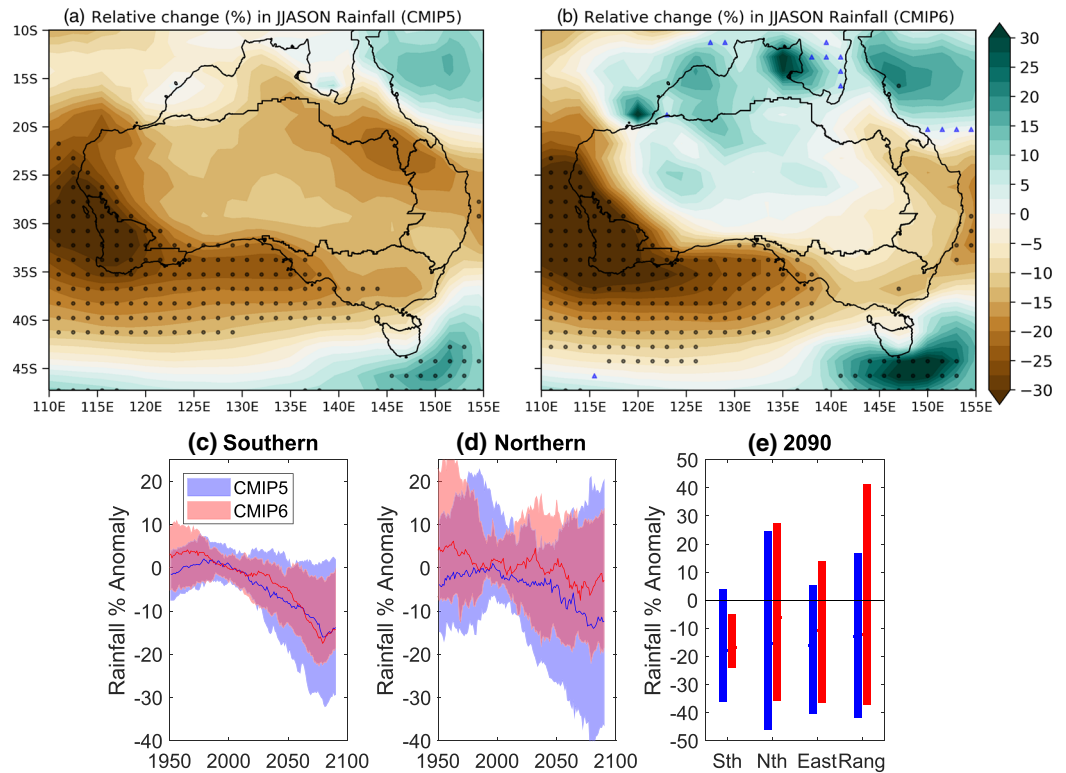


Figure 10. Rainfall projection as for Figure 11 but for JJASON.

The models with an atmospheric resolution greater than 1.2° lat/lon compared to those with coarser resolution (not shown) show no enhanced drying on the slopes of the southern Great Dividing Range as found in downscaling (Grose et al., 2019). This may be because the resolution of CMIP6 models is still notably coarser than CORDEX ($\sim 0.5^\circ$) or other downscaling (~ 5 and ~ 10 km) used in these other studies.

4.3. Daily Extremes

For the precipitation indices there is little difference in projections between CMIP5 and CMIP6 for Australia in terms of spatial pattern and mean difference over land (Figures 11b, 11d, and 11f). However, for temperature extremes (Figures 11a, 11c, and 11e) CMIP6 is decidedly warmer than CMIP5: about 1°C warmer in the coldest night, 1.4°C warmer in the warmest day and >30 days more contributing to warm spells on average over land. The warming is most marked in Northern Australia in TNn, central Australia in TXx, and a general continent-wide warming of WSDI. The temperature results should be treated with some caution as the subset of seven CMIP6 models used in this analysis contains four out of seven models with higher climate sensitivity (ECS of around 4°C or more), so do not represent a balanced sample of the overall ensemble.

In terms of time series and model spread, the temperature indices tend to start off cooler in CMIP6 than CMIP5 but see an acceleration somewhere between 2040 and 2070 (Figure S8) such that by the end of the century the projections are warmer in CMIP6 compared to CMIP5 which is also consistent with the pattern of change seen in Figure 11. Again, the subsample of seven models should be interpreted with caution. Time series of precipitation indices (Figure S8) generally show a more mixed pattern of change. For example, Rx1day is wetter throughout CMIP6 compared to CMIP5 while there are slightly fewer days over 10 mm and almost no discernible difference in consecutive dry days. In all cases, the spread is smaller in CMIP6 compared to CMIP5, but again, this is most likely due to the smaller number of models in the ensemble.

Further details on extremes are considered here based on the 1-year and 10-year ARI. Any increase in temperature extremes will have impacts, and any increase in extremes greater or less than the change in average is useful to understand. Changes in ARI are calculated from a historical period (defined here by 1950 to 1999 for the ARI analysis) to a future period (defined here by 2050 to 2099) using the SSP5-85 pathway. The

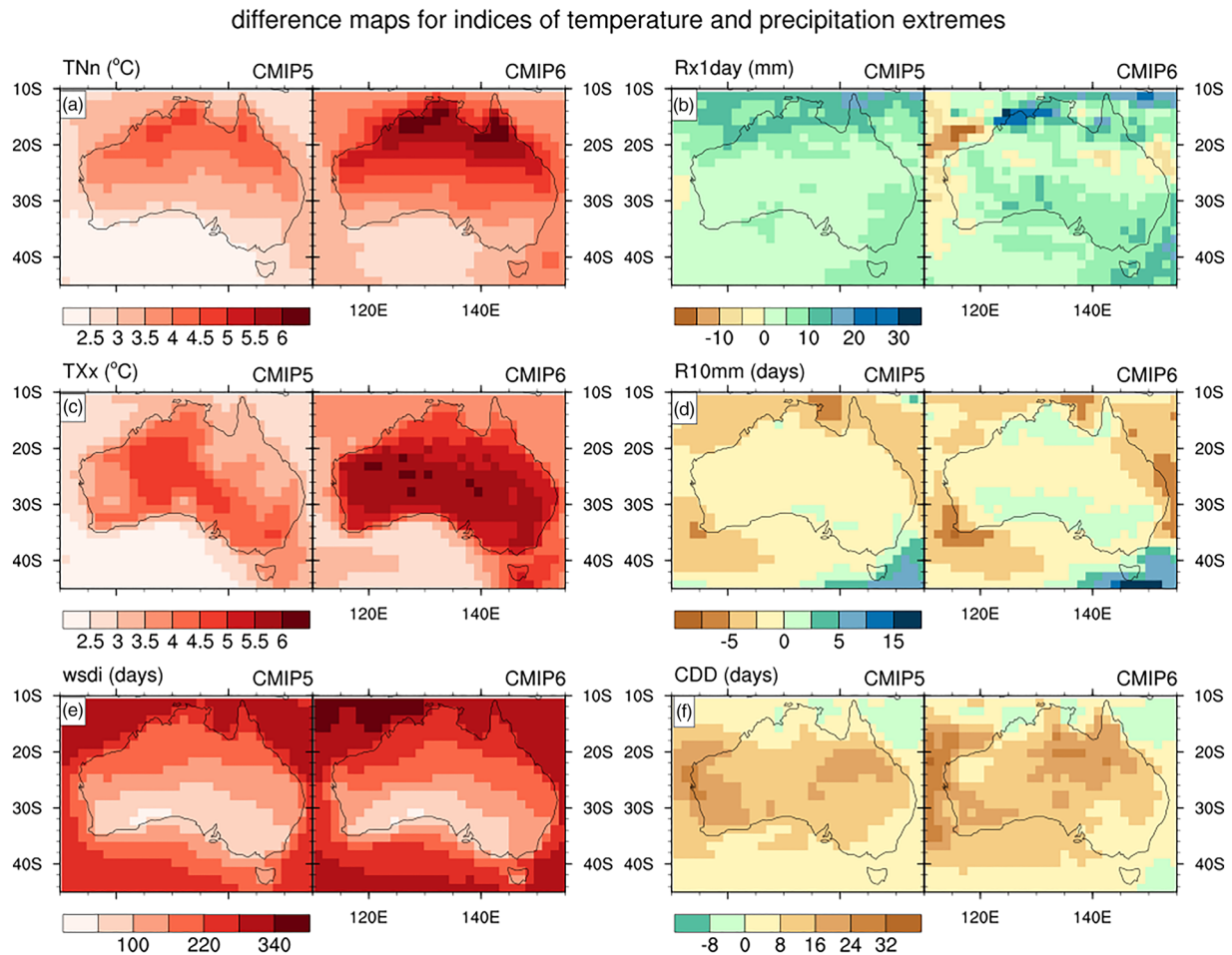


Figure 11. Projected change in six ETCCDI extremes indices (defined in section 2.2) between 1995–2014 and 2080–2099 under RCP8.5/SSP5-85; each panel shows the MMM change in 29 CMIP5 models on the left and MMM change in seven CMIP6 models on the right. The indices and the projected change over the land area of Australia are (a) TNN (CMIP5 3.7 °C, CMIP6 4.7 °C); (b) Rx1day (CMIP5 5.1 mm, CMIP6 5.1 mm); (c) TXx (CMIP5 4.0 °C, CMIP6 5.4 °C); (d) R10mm (CMIP5 0.8 days, CMIP6 0.5 days); (e) wsvd (CMIP5 132.3 days, CMIP6 166.1 days); and (f) cdd (CMIP5 12.9 days, CMIP6 13.0 days).

10-year ARI for tasmax increases by 3.8 °C from 45.0 to 48.8 °C on average over Australia, based on the ensemble mean, which is a similar magnitude change to the case for the 1-year ARI which also increases by 3.8 °C (from 42.8 to 46.6 °C). There is some variation between models, with the range of projected increase being from 2.1 to 6.3 °C for the 10-year ARI and also for the 1 year. The same two models represent these extremes in both cases, with the smaller change for IPSL-CM6A-LR and the larger change for UKESM1-0-LL. In many instances, these temperature ARIs represent events with strong impacts on human health, infrastructure, services, and ecosystems.

Daily rainfall extremes have impacts on flooding, erosion, landslides, infrastructure damage, services disruptions, and much more. The 10-year precipitation ARI increases by 15.5% on average for the ensemble of CMIP6 GCMs used here (with values for individual models ranging from 4.6% to 30.4%), while the 1-year ARI increases by 9.4% (with values ranging from 4.0% to 15.8%). In contrast to the case for extreme tasmax, the projected changes in extreme precipitation are larger for the rarer events (i.e., the 10-year ARI values are larger than the 1-year ARI values). A larger magnitude climate change response for the more intense precipitation events has been reported in previous studies for Australia based on CMIP5 data (CSIRO and BoM 2015) with changes in the 20-year ARI of around 20% to 30% and changes in the 1-year ARI of around 10 to 20% (based on RCP8.5 for the 2080–2099 period as compared to the 1986–2005 period). It is also noted that the resolution of current GCMs, including for CMIP6, is too coarse to adequately simulate severe

thunderstorms and associated extreme convective rainfall events, such that larger magnitude increases than this may be plausible in some cases particularly for short-duration extremes (e.g., hourly extremes associated with super-Clausius Clapeyron processes, Guerreiro et al., 2018).

4.4. ENSO, IOD, and SAM

In both CMIP5 and CMIP6 under high emissions (RCP8.5 and SSP5-85), the intensity of simulated ENSO increases relative to their historical counterparts (Figure S4). The maximum relative increases in Niño-3.4 standard deviation occur in August, indicating that the ENSO growth rate plays a role in this intensification. The increase is larger in CMIP6 under SSP5-85 than in CMIP5 under RCP8.5, presumably because the tropical Pacific mean-state warming is greater in the former (not shown). These results are consistent with those from previous studies based on CMIP5 models (Cai et al., 2014, 2015), which show an increase in the frequency of extreme El Niño and La Niña events under future global warming. However, when the model simulations were individually examined, a substantial number also showed a decrease in ENSO amplitude under strong radiative forcings (Chen et al., 2017; Rashid et al., 2016). Therefore, it will be important to extend the MMM results by looking at simulated ENSO events and their changes under global warming in individual CMIP6 models.

Under high emissions (RCP8.5 and SSP5-85), the location of peak simulated zonal SST variability differs significantly from the historical experiments (Figure S4, bottom panel, lower boxplot). The MMM of available simulations shows that the location of the center of action is displaced further westwards. Peak variability is moved by about 3° longitude based on the MMM of 31 CMIP5 simulations and 7° longitude based on 19 CMIP6 models. This westward displacement of peak variability is larger for CMIP6 models compared to CMIP5 models.

The SAM is projected to become more positive in the future climate under RCP8.5/SSP5-85, with similar results in CMIP5 and CMIP6. All CMIP6 models considered here agree on the sign of this positive trend (Figure S5). Projected trends in SAM have a different seasonal signature than past trends, where the projections feature a maximum increase in late autumn and winter rather than summer. This difference is due to a change in the relative influence of different forcings during the first half of the century, where a recovery of ozone depletion reduces that forcing in summer, whereas an increase in greenhouse gases enhances that forcing in autumn and winter. Given the impact of SAM on rainfall variability shown in previous studies (and well reproduced in the historical CMIP5 and CMIP6 runs, not shown), it seems important to diagnose how much of the projected rainfall change over Australia can result from the projected positive SAM trend. Following the methodology in Lim et al. (2016), we estimate the change in Australian rainfall that is congruent with the change of SAM by regressing rainfall onto detrended SAM in CMIP6 Historical simulations and, for each model, scaling this regression coefficient by the change in SAM from 1995–2014 to 2080–2099. Results suggest that the positive SAM trend mostly contributes to the drying of midlatitudes in winter (e.g., in particular over southwest Western Australia and the southeast tip of Australia) while mitigating the drying over Eastern Australia in that season. In summer, there are suggestions that changes in SAM may enhance the projected wetting of southeast Australia (not shown).

4.5. Dynamic Sea Level

Rising sea levels have major societal impacts through coastal erosion and inundation, wetland flooding, loss of habitats, infiltration of freshwater aquifers, infrastructure damage, and in some cases forced abandonment of coastal settlements. DSL is a notable component of total sea level change and can add or offset the rise and its impacts for any location.

Compared to the CMIP5 ensemble (Figure 7d), the CMIP6 ensemble produces similar features but larger magnitudes of DSL projections over 2080–2099 relative to 1995–2014 (Figure 7e). Off the East Coast, there is a strong north–south contrast of DSL changes, with a smaller (larger) rise in the north (south). A large DSL rise of up to 12 cm in CMIP5 and 14 cm in CMIP6 is projected off the southeast coast of Australia, extending from ~30°S to 45°S. Along and off the Australian south and southwest coasts, there are negative DSL changes of 2 to 4 cm in CMIP5 and 6 to 8 cm in CMIP6. Along the Australian northwest and north coasts, the DSL changes are relatively weak. The contrast between positive DSL changes off East coast and negative DSL changes off south and southwest coasts can be explained by the spin-up of super gyre which links the subtropical Pacific and Indian Ocean circulation (Ridgway & Dunn, 2007; Zhang

et al., 2017). The generally larger DSL projections in CMIP6 than in CMIP5 (Figures 7d and 7e) could be due to the increased climate sensitivity from CMIP5 to CMIP6 (Lyu et al., 2020).

Most of the CMIP5 and CMIP6 models have a typical nominal oceanic resolution of 1° lat/lon and cannot explicitly resolve mesoscale eddies. In contrast, dynamical downscaling with 1/10° lat/lon OGCM reveals some detailed regional features, which are absent in the coarse-resolution CMIP5/6 result (Zhang et al., 2017). For instance, there is a narrow meridional band of high sea levels of around 20 to 30 cm immediately off the southeast coast, extending from ~30°S to 45°S, which is closely related to the poleward shifting and strengthening of the EAC in the future climate. The contrast between the east coast and the south coast is also stronger in the downscaled result (Figure 7f). Using downscaled results as a reference, there is some improvement in the CMIP6 DSL projections, but CMIP6 still cannot resolve some finer-scale features around Australia especially in the EAC and its extension region.

5. Conclusions

This paper presents evaluation and projections information about climate change in Australia from the available CMIP6 ensemble, placed in the context of information from the CMIP5 ensemble. It is important to reiterate here that differences between the two ensembles are due to several factors. Differences between CMIP5 and CMIP6 in their evaluation compared to observations could in part be due to the sophistication of the models, for example, the proportion of ESMs, the representation of aerosol effects, model resolution, and parameterization improvements. Differences in the projections are due in part to issues such as model climate sensitivity to greenhouse gas concentrations and some contribution from differences in the greenhouse gases and aerosol forcing scenarios in the RCPs and the new SSPs. We do not attempt to attribute the ensemble differences to specific processes or mechanisms, instead focusing on reporting the differences across a range of metrics.

We find a number of differences between the two ensembles, highlighted and discussed in detail in the previous sections. Incremental improvements in the historical mean state is found in the CMIP6 ensemble compared to CMIP5; however, significant regional biases remain, for example, over the Maritime Continent and the western equatorial Pacific. While the range of strengths between important teleconnections between large-scale climate drivers and Australian rainfall is marginally improved (i.e., reduced), in general, the strength of these teleconnections is too weak. The simulated temperature and rainfall extremes are similar in the two ensembles, with the exception of the projected change in temperature extremes, which is larger in CMIP6, potentially due to increased climate sensitivity. The simulation of MHWs and DSL is found to be improved, although the projections remain similar between the ensembles.

The projections of Australian mean and extreme climate variables are broadly similar in CMIP5 and CMIP6 in terms of directions of change and spatial distributions. Both ensembles project warming temperatures and increases in hot extremes proportional to the greenhouse forcing, but CMIP6 provides a hotter high end to projections beyond 2050, including a change of over 6 °C mean annual temperature since the preindustrial era by 2100 under a high emissions scenario. Unless subsequent research and evidence can be used to confidently reject these projections, it must be accepted as a credible finding.

The higher end of the range of temperature projections in CMIP6, with a corresponding rise in heat extremes, has many implications for the ecological and socioeconomic impact of projected climate change under a high emissions scenario. Greater impacts on terrestrial and marine ecosystems, human health, the economy and society are projected at the high end in CMIP6 compared to CMIP5. Or framed differently, CMIP6 indicates a lower magnitude of total greenhouse gas emissions is required for all models to be below a given warming threshold (e.g., 2 °C) than CMIP5 produced.

Both CMIP5 and CMIP6 project a significant drying of southwest Australia in the cool season and less certain or less significant rainfall projections elsewhere. The CMIP6 ensemble so far suggests there is greater confidence in rainfall decrease in Southern Australia in the austral cool season and a constrained range of rainfall change in the wetter end for Northern Australia during the austral warm season than in CMIP5. If this result is maintained as more models are added, these projections will be one line of evidence for more targeted and specific adaptation actions required in the relation to the mean rainfall of Australia.

In time, the full CMIP6 ensemble will become available; however, using the available archive, we have already shown in the present study some of the apparent improvements as well as some notable similarities between the state-of-the-art model projections compared to the previous generation. This information should inform regionally relevant climate change projections for Australia.

Acknowledgments

We acknowledge the support of Australian Government's National Environmental Science Programme's Earth Systems and Climate Change Hub and the Australian Research Council Centre of Excellence for Climate Extremes (Grant CE170100023). K.L. and X.Z. were also supported by Centre for Southern Hemisphere Oceans Research (CSHOR), a joint research center between QNLM China and CSIRO Australia. We thank Martin Dix from CSIRO for calculating the ECS indices. We acknowledge the World Climate Research Programme's Working Group on Coupled Modelling, which is responsible for CMIP, and we thank the climate modeling groups for producing and making available their model output. CMIP5 and CMIP6 model outputs were made available with the assistance of resources from the National Computational Infrastructure (NCI), which is supported by the Australian Government. NOAA High Resolution SST data provided by the NOAA/OAR/ESRL PSD, Boulder, Colorado, USA, from their website at <https://www.esrl.noaa.gov/psd/>. All the data used in the analysis are publicly available and can be downloaded at <https://doi.org/10.5281/zenodo.3676121>.

References

- Adler, R. F., Huffman, G. J., Chang, A., Ferraro, R., Xie, P. P., Janowiak, J., et al. (2003). The Version-2 Global Precipitation Climatology Project (GPCP) Monthly Precipitation Analysis (1979–present). *Journal of Hydrometeorology*, *4*(6), 1147–1167. [https://doi.org/10.1175/1525-7541\(2003\)004<1147:TVGPCP>2.0.CO;2](https://doi.org/10.1175/1525-7541(2003)004<1147:TVGPCP>2.0.CO;2)
- Bellenger, H., Guilyardi, E., Leloup, J., Lengaigne, M., & Vialard, J. (2014). ENSO representation in climate models: From CMIP3 to CMIP5. *Climate Dynamics*, *42*(7–8), 1999–2018. <https://doi.org/10.1007/s00382-013-1783-z>
- Brown, J., Moise, A., & Colman, R. (2013a). The South Pacific Convergence Zone in CMIP5 simulations of historical and future climate. *Climate Dynamics*, *41*(7–8), 2179–2197. <https://doi.org/10.1007/s00382-012-1591-x>
- Brown, J. N., Langlais, C., & Sen Gupta, A. (2015). Projected sea surface temperature changes in the equatorial Pacific relative to the Warm Pool edge. *Deep Sea Research Part II: Topical Studies in Oceanography*, *113*, 47–58. <https://doi.org/10.1016/j.dsr2.2014.10.022>
- Brown, J. N., Maes, C., Sen Gupta, A., Matear, R. J., Cravatte, S., Langlais, C., & participants, O. W. (2013). Reinvigorating research on the Western Pacific Warm Pool—First workshop. *CLIVAR exchanges doi*, *119*(1), 147–161. <https://doi.org/10.1007/s10584-012-0603-5>
- Brown, J. R., Moise, A. F., Colman, R., & Zhang, H. (2016). Will a warmer world mean a wetter or drier Australian monsoon? *Journal of Climate*, *29*(12), 4577–4596. <https://doi.org/10.1175/JCLI-D-15-0695.1>
- Cai, W., Borlace, S., Lengaigne, M., Van Rensch, P., Collins, M., Vecchi, G., et al. (2014). Increasing frequency of extreme El Niño events due to greenhouse warming. *Nature Climate Change*, *4*(2), 111–116. <https://doi.org/10.1038/nclimate2100>
- Cai, W., & Cowan, T. (2013). Why is the amplitude of the Indian Ocean Dipole overly large in CMIP3 and CMIP5 climate models? *Geophysical Research Letters*, *40*(6), 1200–1205. <https://doi.org/10.1002/grl.50208>
- Cai, W., Sullivan, A., & Cowan, T. (2009). Rainfall teleconnections with Indo-Pacific variability in the WCRP CMIP3 models. *Journal of Climate*, *22*(19), 5046–5071. <https://doi.org/10.1175/2009JCLI2694.1>
- Cai, W., van Rensch, P., Cowan, T., & Hendon, H. H. (2011). Teleconnection pathways of ENSO and the IOD and the mechanisms for impacts on Australian rainfall. *Journal of Climate*, *24*(15), 3910–3923. <https://doi.org/10.1175/2011JCLI4129.1>
- Cai, W., Wang, G., Santoso, A., McPhaden, M. J., Wu, L., Jin, F. F., et al. (2015). Increased frequency of extreme La Niña events under greenhouse warming. *Nature Climate Change*, *5*(2), 132–137. <https://doi.org/10.1038/nclimate2492>
- Chen, L., Li, T., Yu, Y., & Behera, S. K. (2017). A possible explanation for the divergent projection of ENSO amplitude change under global warming. *Climate Dynamics*, *49*(11–12), 3799–3811. <https://doi.org/10.1007/s00382-017-3544-x>
- Christensen, J. H., Kanikicharla, K. K., Aldrian, E., An, S. I., Cavalcanti, I. F., De Castro, M., et al. (2013). Climate phenomena and their relevance for future regional climate change. In T. F. Stocker, D. Qin, G.-K. Plattner, et al. (Eds.), *Climate Change 2013: The Physical Science Basis. Contribution of Working Group I to the Fifth Assessment Report of the Intergovernmental Panel on Climate Change*, (pp. 1217–1308). Cambridge, United Kingdom and New York, NY, USA: Cambridge University Press. <https://doi.org/10.1017/CBO9781107415324.028>
- Collins, M., Knutti, R., Arblaster, J., Dufresne, J. L., Fichefet, T., Friedlingstein, P., et al. (2013). Long-term climate change: Projections, commitments and irreversibility. In T. F. Stocker, D. Qin, G.-K. Plattner, et al. (Eds.), *Climate Change 2013: The Physical Science Basis. Contribution of Working Group I to the Fifth Assessment Report of the Intergovernmental Panel on Climate Change* (pp. 1029–1136). Cambridge, United Kingdom and New York, NY, USA: Cambridge University Press. <https://doi.org/10.1017/CBO9781107415324.024>
- Colman, R. A., Moise, A. F., & Hanson, L. I. (2011). Tropical Australian climate and the Australian monsoon as simulated by 23 CMIP3 models. *Journal of Geophysical Research-Atmospheres*, *116*(D10), D10116. <https://doi.org/10.1029/2010JD015149>
- CSIRO and Bureau of Meteorology (2007). Climate change in Australia. *Technical Report*. Australia. www.climatechangeinaustralia.gov.au
- CSIRO and Bureau of Meteorology (2015). Climate change in Australia, Technical Report. Melbourne Australia. www.climatechangeinaustralia.gov.au
- Dee, D. P., Uppala, S. M., Simmons, A. J., Berrisford, P., Poli, P., Kobayashi, S., et al. (2011). The ERA-Interim reanalysis: Configuration and performance of the data assimilation system. *Quarterly Journal of the Royal Meteorological Society*, *137*(656), 553–597. <https://doi.org/10.1002/qj.828>
- Eyring, V., Bony, S., Meehl, G. A., Senior, C. A., Stevens, B., Stouffer, R. J., & Taylor, K. E. (2016). Overview of the Coupled Model Intercomparison Project Phase 6 (CMIP6) experimental design and organization. *Geoscientific Model Development*, *9*(5), 1937–1958. <https://doi.org/10.5194/gmd-9-1937-2016>
- Flato, G., & co-authors (2013). Evaluation of climate models. In T. F. Stocker, D. Qin, G.-K. Plattner, et al. (Eds.), *Climate Change 2013: The Physical Science Basis. Contribution of Working Group I to the Fifth Assessment Report of the Intergovernmental Panel on Climate Change*, (pp. 741–866). Cambridge, United Kingdom and New York, NY, USA: Cambridge University Press. <https://doi.org/10.1017/CBO9781107415324.020>
- Forster, P. M., Maycock, A. C., McKenna, C. M., & Smith, C. J. (2019). Latest climate models confirm need for urgent mitigation. *Nature Climate Change*. <https://doi.org/10.1038/s41558-019-0660-0>
- Frölicher, T. L., Fischer, E. M., & Gruber, N. (2018). Marine heatwaves under global warming. *Nature*, *560*(7718), 360–364. <https://doi.org/10.1038/s41586-018-0383-9>
- Gottelman, A., Hannay, C., Bacmeister, J. T., Neale, R. B., Pendergrass, A. G., Danabasoglu, G., et al. (2019). High climate sensitivity in the Community Earth System Model Version 2 (CESM2). *Geophysical Research Letters*, *46*, 8329–8337. <https://doi.org/10.1029/2019GL083978>
- Gong, D., & Wang, S. (1999). Definition of Antarctic oscillation index. *Geophysical Research Letters*, *26*(4), 459–462. <https://doi.org/10.1029/1999GL900003>
- Gregory, J. M., Andrews, T., Ceppi, P., Mauritsen, T., & Webb, M. J. (2019). How accurately can the climate sensitivity to CO₂ be estimated from historical climate change? *Climate Dynamics doi*, *54*(1–2), 129–157. <https://doi.org/10.1007/s00382-019-04991-y>

- Gregory, J. M., Ingram, W. J., Palmer, M. A., Jones, G. S., Stott, P. A., Thorpe, R. B., et al. (2004). A new method for diagnosing radiative forcing and climate sensitivity. *Geophysical Research Letters*, *31*, L03205. <https://doi.org/10.1029/2003GL018747>
- Grose, M. R., Brown, J. N., Narsey, S., Brown, J. R., Murphy, B. F., Langlais, C., et al. (2014). Assessment of the CMIP5 global climate model simulations of the western tropical Pacific climate system and comparison to CMIP3. *International Journal of Climatology*, *34*(12), 3382–3399. <https://doi.org/10.1002/joc.3916>
- Grose, M. R., Colman, R., Bhend, J., & Moise, A. F. (2016). Limits to global and Australian temperature change this century based on expert judgment of climate sensitivity. *Climate Dynamics*, *48*(9–10), 3325–3339. <https://doi.org/10.1007/s00382-016-3269-2>
- Grose, M. R., Syktus, J., Thatcher, M., Evans, J. P., Ji, F., Rafter, T., & Remenyi, T. (2019). The role of topography on projected rainfall change in mid-latitude mountain regions. *Climate Dynamics* doi, *53*(5–6), 3675–3690. <https://doi.org/10.1007/s00382-019-04736-x>
- Guerreiro, S. B., Fowler, H. J., Barbero, R., Westra, S., Lenderink, G., Blenkinsop, S., et al. (2018). Detection of continental-scale intensification of hourly rainfall extremes. *Nature Climate Change*, *8*, 803–807. <https://doi.org/10.1038/s41558-018-0245-3>
- Hendon, H. H., Lim, E.-P., & Ngyuen, H. (2014). Variations of subtropical precipitation and circulation associated with the Southern Annular Mode. *Journal of Climate*, *27*(9), 3446–3460. <https://doi.org/10.1175/JCLI-D-13-00550.1>
- Hendon, H. H., Thompson, D. W. J., & Wheeler, M. C. (2007). Australian rainfall and surface temperature variations associated with the Southern Hemisphere annular mode. *Journal of Climate*, *20*(11), 2452–2467. <https://doi.org/10.1175/JCLI4134.1>
- Hobday, A. J., Alexander, L. V., Perkins, S. E., Smale, D. A., Straub, S. C., Oliver, E. C., et al. (2016). A hierarchical approach to defining marine heatwaves. *Progress in Oceanography*, *141*, 227–238. <https://doi.org/10.1016/j.pocean.2015.12.014>
- Holbrook, N. J., & Johnson, J. E. (2014). Climate change impacts and adaptation of commercial marine fisheries in Australia: A review of the science. *Climatic Change*, *124*(4), 703–715. <https://doi.org/10.1007/s10584-014-1110-7>
- IPCC (2007). *Contribution of Working Group I to the Fourth Assessment Report of the Intergovernmental Panel on Climate Change*, 2007. Cambridge, United Kingdom and New York, NY, USA: Cambridge University Press.
- IPCC (2013). Climate Change 2013: The Physical Science Basis. In T. F. Stocker, D. Qin, G.-K. Plattner, et al. (Eds.), *Contribution of Working Group I to the Fifth Assessment Report of the Intergovernmental Panel on Climate Change* (pp. 1256) Cambridge, UK, and New York, NY, USA: Cambridge University Press.
- Johnson, J. E., & Holbrook, N. J. (2014). Adaptation of Australia's marine ecosystems to climate change: Using science to inform conservation management. *International Journal of Ecology*, *2014*, 12.
- Jones, D. A., Wang, W., & Fawcett, R. (2009). High-quality spatial climate datasets for Australia. *Australian Meteorological and Oceanographic Journal*, *58*(04), 233–248. <https://doi.org/10.22499/2.5804.003>
- Lee, T., Waliser, D. E., Li, J.-L. F., Landerer, F. W., & Gierach, M. M. (2013). Evaluation of CMIP3 and CMIP5 wind stress climatology using satellite measurements and atmospheric reanalysis products. *Journal of Climate*, *26*(16), 5810–5826. <https://doi.org/10.1175/JCLI-D-12-00591.1>
- Li, G., Jian, Y., Yang, S., Du, Y., Wang, Z., Li, Z., et al. (2019). Effect of excessive equatorial Pacific cold tongue bias on the El Niño-Northwest Pacific summer monsoon relationship in CMIP5 multi-model ensemble. *Climate Dynamics*, *52*(9–10), 6195–6212. <https://doi.org/10.1007/s00382-018-4504-9>
- Li, G., & Xie, S.-P. (2014). Tropical biases in CMIP5 multi-model ensemble: The excessive equatorial Pacific cold tongue and double ITCZ problems. *Journal of Climate*, *27*(4), 1765–1780. <https://doi.org/10.1175/JCLI-D-13-00337.1>
- Li, G., Xie, S.-P., Du, Y., & Luo, Y. (2016). Effects of excessive equatorial cold tongue bias on the projections of tropical Pacific climate change. Part I: The warming pattern in CMIP5 multi-model ensemble. *Climate Dynamics*, *47*(12), 3817–3831. <https://doi.org/10.1007/s00382-016-3043-5>
- Lim, E.-P., Hendon, H. H., Arblaster, J. M., Delage, F., Nguyen, H., Min, S. K., & Wheeler, M. C. (2016). The impact of the Southern Annular Mode on future changes in Southern Hemisphere rainfall. *Geophysical Research Letters*, *43*(13), 7160–7167. <https://doi.org/10.1002/2016GL069453>
- Liu, L., Xie, S.-P., Zheng, X.-T., Li, T., Du, Y., Huang, G., & Yu, W.-D. (2014). Indian Ocean variability in the CMIP5 multi-model ensemble: The zonal dipole mode. *Climate Dynamics*, *43*(5–6), 1715–1730. <https://doi.org/10.1007/s00382-013-2000-9>
- Lyu, K., Zhang, X., & Church, J. A. (2020). Regional dynamic sea level simulations in the CMIP5 and CMIP6 models: Mean biases, future projections, and their linkages. *Journal of Climate*. under revision
- Maximenko, N., Niiler, P., Centurioni, L., Rio, M.-H., Melnichenko, O., Chambers, D., et al. (2009). Mean dynamic topography of the ocean derived from satellite and drifting buoy data using three different techniques. *Journal of Atmospheric and Oceanic Technology*, *26*(9), 1910–1919. <https://doi.org/10.1175/2009JTECHO672.1>
- Mechoso, C., Robertson, A. W., Barth, N., Davey, M. K., Delecluse, P., Gent, P. R., et al. (1995). The seasonal cycle over the tropical Pacific in coupled ocean-atmosphere general circulation models. *Monthly Weather Review*, *123*(9), 2825–2838. [https://doi.org/10.1175/1520-0493\(1995\)123<2825:TSCOTT>2.0.CO;2](https://doi.org/10.1175/1520-0493(1995)123<2825:TSCOTT>2.0.CO;2)
- Meinshausen, M., Nicholls, Z., Lewis, J., Gidden, M. J., Vogel, E., Freund, M., et al. (2019). The SSP greenhouse gas concentrations and their extensions to 2500. *Geoscientific Model Development Discussion*, *2019*, 1–77. <https://doi.org/10.5194/gmd-2019-222>
- Meyers, G., McIntosh, P., Pigot, L., & Pook, M. (2007). The years of El Niño, La Niña, and interactions with the tropical Indian Ocean. *Journal of Climate*, *20*(13), 2872–2880. <https://doi.org/10.1175/JCLI4152.1>
- NCC-Editorial (2019). The CMIP6 landscape. *Nature Climate Change*, *9*, 727–727.
- Oliver, E. C. J., Burrows, M. T., Donat, M. G., Sen Gupta, A., Alexander, L. V., Perkins-Kirkpatrick, S. E., et al. (2019). Projected marine heatwaves in the 21st century and the potential for ecological impact. *Frontiers in Marine Science*, *6*, 734. <https://doi.org/10.3389/fmars.2019.00734>
- Oliver, E. C. J., Donat, M. G., Burrows, M. T., Moore, P. J., Smale, D. A., Alexander, L. V., et al. (2018). Longer and more frequent marine heatwaves over the past century. *Nature Communications*, *9*(1), 1324. <https://doi.org/10.1038/s41467-018-03732-9>
- O'Neill, B. C., Tebaldi, C., Van Vuuren, D. P., Eyring, V., Friedlingstein, P., Hurtt, G., et al. (2016). The Scenario Model Intercomparison Project (ScenarioMIP) for CMIP6. *Geoscientific Model Development*, *9*(9), 3461–3482. <https://doi.org/10.5194/gmd-9-3461-2016>
- Pilo, G. S., Holbrook, N. J., Kiss, A. E., & Hogg, A. M. (2019). Sensitivity of marine heatwave metrics to ocean model resolution. *Geophysical Research Letters*, *46*(24), 14604–14612. <https://doi.org/10.1029/2019GL084928>
- Rashid, H. A., Hirst, A. C., & Marsland, S. J. (2016). An atmospheric mechanism for ENSO amplitude changes under an abrupt quadrupling of CO₂ concentration in CMIP5 models. *Geophysical Research Letters*, *43*(4), 1687–1694. <https://doi.org/10.1002/2015gl066768>
- Raupach, M. R., Briggs, P. R., Haverd, V., King, E. A., Paget, M., & Trudinger, C. M. (2009). *Australian Water Availability Project (AWAP), final report for Phase 3*, (p. 67). CSIRO Marine and Atmospheric Research: Canberra, Australia.

- Rayner, N. A., Parker, D. E., Horton, E. B., Folland, C. K., Alexander, L. V., Rowell, D. P., et al. (2003). Global analyses of sea surface temperature, sea ice, and night marine air temperature since the late nineteenth century. *Journal of Geophysical Research-Atmospheres*, *108*(D14), 4407. <https://doi.org/10.1029/2002JD002670>
- Reynolds, R. W., Smith, T. M., Liu, C., Chelton, D. B., Casey, K. S., & Schlax, M. G. (2007). Daily high-resolution-blended analyses for sea surface temperature. *Journal of Climate*, *20*(22), 5473–5496. <https://doi.org/10.1175/2007JCLI1824.1>
- Ridgway, K. R., & Dunn, J. R. (2007). Observational evidence for a Southern Hemisphere oceanic supergyre. *Geophysical Research Letters*, *34*(13), n/a. <https://doi.org/10.1029/2007GL030392>
- Risbey, J. S., Pook, M. J., McIntosh, P. C., Wheeler, M. C., & Hendon, H. H. (2009). On the remote drivers of rainfall variability in Australia. *Monthly Weather Review*, *137*(10), 3233–3253. <https://doi.org/10.1175/2009MWR2861.1>
- Schurer, A. P., Mann, M. E., Hawkins, E., Tett, S. F. B., & Hegerl, G. C. (2017). Importance of the pre-industrial baseline for likelihood of exceeding Paris goals. *Nature Climate Change*, *7*(8), 563–567. <https://doi.org/10.1038/nclimate3345>
- Sellar, A. A., Jones, C. G., Mulcahy, J., Tang, Y., Yool, A., Wiltshire, A., et al. (2019). UKESM1: Description and evaluation of the UK Earth System Model. *Journal of Advances in Modelling Earth Systems*, *11*(12), 4513–4558. <https://doi.org/10.1029/2019MS001739>
- Smale, D. A., Wernberg, T., Oliver, E. C., Thomsen, M., Harvey, B. P., Straub, S. C., et al. (2019). Marine heatwaves threaten global biodiversity and the provision of ecosystem services. *Nature Climate Change*, *9*(4), 306–312. <https://doi.org/10.1038/s41558-019-0412-1>
- Taylor, K. E., Stouffer, R. J., & Meehl, G. A. (2012). An overview of CMIP5 and the experiment design. *Bulletin of the American Meteorological Society*, *93*(4), 485–498. <https://doi.org/10.1175/BAMS-D-11-00094.1>
- Thompson, D. W. J., & Wallace, J. M. (2000). Annular modes in the extratropical circulation. *Part I: Month-to-month variability*. *Journal of Climate*, *13*, 1000–1016.
- Toh, Y. Y., Turner, A. G., Johnson, S. J., & Holloway, C. E. (2018). Maritime continent seasonal climate biases in AMIP experiments of the CMIP5 multi-model ensemble. *Climate Dynamics*, *50*(3-4), 777–800. <https://doi.org/10.1007/s00382-017-3641-x>
- van Vuuren, D., Edmonds, J., Kainuma, M., Riahi, K., Thomson, A., Hibbard, K., et al. (2011). The representative concentration pathways: An overview. *Climatic Change*, *109*(1-2), 5–31. <https://doi.org/10.1007/s10584-011-0148-z>
- Voosen, P. (2019). New climate models predict a warming surge. *Science News*. <https://doi.org/10.1126/science.aax7217>
- Ying, J., Huang, P., Lian, T., & Tan, H. (2019). Understanding the effect of an excessive cold tongue bias on projecting the tropical Pacific SST warming pattern in CMIP5 models. *Climate Dynamics*, *52*(3-4), 1805–1818. <https://doi.org/10.1007/s00382-018-4219-y>
- Zhang, X., Alexander, L., Hegerl, G. C., Jones, P., Klein Tank, A., Peterson, T. C., et al. (2011). Indices for monitoring changes in extremes based on daily temperature and precipitation data. *WIREs Climate Change*, *2*(6), 851–870. <https://doi.org/10.1002/wcc.147>
- Zhang, X., Church, J. A., Monselesan, D., & McInnes, K. L. (2017). Sea level projections for the Australian region in the 21st century. *Geophysical Research Letters*, *44*(16), 8481–8491. <https://doi.org/10.1002/2017GL074176>